Loss of sea ice and intermittent winds alter distributions and diet resources of young forage fish in the Chukchi Sea

[*1,2]Esther D. Goldstein, [3]Ryan M. McCabe, [4]Matthew C. Rogers, [2,5]Alison L. Deary, [2,6]Janet T. Duffy-Anderson

[1]NOAA, Alaska Fisheries Science Center, Resource Ecology and Fisheries Management Division, 7600 Sand Point Way NE, Seattle, Washington, 98115, USA

[2]NOAA, Alaska Fisheries Science Center, Resource Assessment and Conservation Engineering Division, 7600 Sand Point Way NE, Seattle, Washington, 98115, USA

[3]NOAA, Pacific Marine Environmental Laboratory, 7600 Sand Point Way NE, Seattle, Washington, 98115, USA

[4]NOAA, Alaska Fisheries Science Center, Auke Bay Laboratories, 17109 Pt. Lena Loop, Juneau, Alaska, 99801, USA

[5]U.S. Fish and Wildlife Service, Abernathy Fish Technology Center, 1440 Abernathy Creek Road, Longview, Washington, 98632, USA

[6]Gulf of Maine Research Institute, 350 Commercial St., Portland, Maine, 04101, USA

Corresponding author: Esther.Goldstein@noaa.gov

Keywords: Compound-specific stable isotope, sea ice, Arctic, forage fish, copepod, *Boreogadus saida*, *Eleginus gracilis*, Chukchi Sea

Abstract

Loss of sea ice alters habitat for organisms that function as energetic links in Arctic food webs. To address the impacts of such changes on lower trophic levels we focus on forage fish during the early life stages (polar cod: *Boreogadus saida* and saffron cod: *Eleginus gracilis*) and copepods (*Calanus* spp. and *Pseudocalanus* spp.) in the Chukchi Sea with differing reliance on sea ice environments. We assess distributions throughout years of varying ice extent (2010–2013, 2015, 2017–2018) and diet resources during unprecedented warm years (2017, 2018) using stable isotope analyses (bulk $\delta^{13}C$ and $\delta^{15}N$ and $\delta^{13}C$ compound-specific isotope analysis of amino acids). *Calanus* spp. and polar cod were found at relatively higher latitudes in closer proximity to recent sea ice, whereas saffron cod were rare and *Pseudocalanus* spp. were ubiquitous. Polar cod juveniles, but not larvae, were more common in open water, suggesting that low ice and northward ocean currents interact to influence juvenile distributions. Low summer sea ice also coincided with northward expansion of warm Pacific-origin water across the shelf. Stable isotope $\delta^{13}C$ values reflected this latitudinal variation in water masses as well as inshore-offshore gradients due to convergence of ocean currents. When summer sea ice was absent during 2017, juvenile polar cod were dispersed across the shelf, abundances were low for both copepod taxa, isotopic niche was reduced for polar cod, and carbon sources for some larval polar cod reflected boreal-associated phytoplankton. Distributions and isotopic patterns suggest that under low ice conditions, along-shelf wind reversals and weak currents can lead to dominance of Pacific-origin water, mixing of organisms from various source locations, and reductions in sea ice-influenced environments. Northward expansion of subarctic water masses and organisms across the Chukchi shelf alters basal resources for lower trophic levels and modifies pelagic habitats to more uniformly resemble lower latitude marine ecosystems.

1. Introduction

Arctic warming leads to reductions in sea ice and has cascading impacts on marine ecosystems such as altering the phenology and magnitude of algal blooms (Ji et al., 2013) and the composition and distribution of organisms (Frainer et al., 2017). Sea ice algal blooms contribute to seasonal primary production that forms the base of Arctic food webs (Griffith et al., 2019) and typically occur during the spring when ice retreats (Tedesco et al., 2019). An extended ice-free period may alter the timing of blooms and subsequent pelagic productivity pulses (Ji et al., 2013; Wassmann and Reigstad, 2011), impacting trophic relationships and shifting Arctic food webs from ice algae (sympagic) to phytoplankton (Kędra et al., 2019; Kortsch et al., 2015). For example, forage fish and copepods rely on sea ice habitats and ice algal productivity to varying degrees among seasons and throughout ontogeny, and are important links between primary producers and upper trophic levels (Fortier et al., 1995; Koch et al. 2023; Søreide et al., 2010).

Loss of ice can coincide with other physical processes that exacerbate ecosystem changes. Arctic continental shelf habitats connect subarctic environments with the high Arctic and have undergone drastic declines in sea ice in the past few decades (Grebmeier 2012). In the US Arctic, ocean currents through Bering Strait that connect the North Pacific Ocean with the shelf habitats of the Chukchi Sea (henceforth Chukchi) are typically northward, with synoptic-scale variations in water velocity forced by winds (Danielson et al., 2014; Woodgate et al., 2005). Shifts in the direction or magnitude of winds or currents can affect temperatures, alter water mass distributions (Danielson et al. 2017), increase the duration of open water (Serreze and Barry, 2011), and expand distributions of subarctic plankton communities (Axler et al. 2023; Spear et al., 2019). Warming also increases stratification and restricts nutrient delivery to the

photic zone, favoring smaller plankton such as those found at lower latitudes (Wassmann and Reigstad, 2011). Thus, in addition to loss of ice, the transport of warm Pacific-origin water into the US Arctic modifies the shelf habitat to resemble subarctic marine ecosystems.

Unprecedented warming in the Arctic warrants an understanding of the impacts of loss of sea ice on pelagic habitats, primary producers, and the potential for such changes to impact marine food webs and ecosystems. Stable isotope analyses from animal tissues provide a method to detect environmental change and shifts in basal resources that propagate across trophic levels (Marsh et al., 2017; Schell et al., 1998). Generally, $\delta^{13}C$ ($\delta^{13}C$; δ notation is the ratio of heavy to light isotopes relative to a standard) is indicative of carbon sources or spatial patterns in isotope distributions (isoscapes); whereas nitrogen stable isotopes ($\delta^{15}N$) relate to trophic position due to ^{15}N enrichment from prey to consumer (Jackson et al., 2011). However, disentangling the specific drivers of variability can be challenging using bulk tissue analyses because $\delta^{15}N$ and $\delta^{13}C$ are influenced by physiological and biochemical processes that impact trophic fractionation (Larsen et al., 2013). $\delta^{13}C$ from compound-specific isotope analysis of amino acids (CSIAA) can better identify shifts in basal carbon resources utilized by an organism. Essential amino acids (AA) can only be synthesized by bacteria, fungi, and photoautotrophs and are routed from the diet directly into the tissue of the consumer, thereby minimizing trophic fractionation and the need for isotopic baseline measurements (Larsen et al., 2013; McMahon et al., 2010).

Bulk isotope analyses paired with CSIAA can therefore be used to detect environmental change associated with loss of sea ice including shifts in trophic position, variation in water masses (Marsh et al., 2017), and changes in food web basal resources (Vane et al. 2023). Decadal declines in carbon stable isotopes in the Arctic have been attributed to global anthropogenic inputs of carbon dioxide (de la Vega et al., 2019), but isoscapes are influenced by several factors.

Carbon isotopes can signal inputs to marine systems from land based sources and increased riverine flow that is generally ^{13}C-depleted compared to oceanic sources (de la Vega et al., 2019). Proliferation and growth of primary producers that utilize the dissolved CO_2 pool during blooms can lead to ^{13}C enrichment (higher ratio of ^{13}C to ^{12}C; de la Vega et al., 2019; Søreide et al., 2013). Basal carbon sources such as bacteria, phytoplankton, or sea ice-associated algae also alter $\delta^{13}C$ (Zinkann et al. 2022), signifying impacts of sea ice decline and warming that may cascade throughout Arctic food webs (Koch et al., 2023; Vane et al. 2023). Accordingly, stable isotopes measured from lower trophic level organisms such as copepods and forage fish, that link primary producers and upper trophic levels, can provide an indicator of changes in basal food web resources and marine ecosystems.

Copepod and forage fish taxa that are important for energy transfer in Arctic food webs are differentially linked to sympagic habitats, suggesting sensitivities to loss of sea ice for some species. Large-bodied *Calanus* spp. copepods provide lipid-rich prey items for fish (Gray et al., 2016), sea birds, and mammals (Søreide et al., 2010, Rogachev et al., 2008). Both *C. glacialis* and *C. marshallae* are found in the Chukchi and are challenging to differentiate, but *C. glacialis* is the predominant species in the region (Spear et al., 2019; Hopcroft et al., 2010). The life cycle of *C. glacialis* is coupled with the sea ice algal bloom to support the energetic demands of reproduction, and the subsequent phytoplankton bloom to provide food for offspring (Leu et al., 2011; Søreide et al., 2010). *Pseudocalanus* spp. copepods have a smaller body size than *Calanus* spp., but they are an important component of the zooplankton community due to high turnover and biomass (Ershova et al., 2017). The genera is comprised of species found throughout the Arctic and North Pacific that are virtually indistinguishable, with some species associated with sea ice (Ershova et al., 2017). Thus, the genera as a whole is less coupled than *Calanus* spp. to

sympagic habitats. Polar cod (*Boreogadus saida*) is the most prevalent forage fish species in the Chukchi, but co-occurring gadids, including saffron cod (*Eleginus gracilis*), potentially play a similar nodal role in Arctic food webs (Mueter et al. 2016). Polar cod serve as a critical link between zooplankton and higher trophic levels such as birds and mammals (Hop and Gjøsæter, 2013). Eggs hatch under the ice (Bouchard and Fortier, 2008) and larvae primarily prey on copepod eggs and nauplii (Bouchard and Fortier, 2020) before transitioning to a broader diet that includes *C. glacialis* and non-copepod prey (Gray et al., 2016; Michaud et al., 1996). Saffron cod are often in warmer waters than polar cod, and young fish are generally closer to shore (Vestfals et al., 2019). Warmer temperatures are also more favorable for saffron cod growth and condition compared to polar cod (Laurel et al., 2016), suggesting that a warming Arctic may be more detrimental to polar cod.

Warming temperatures and loss of sea ice are expected to modify pelagic habitats and food webs in the Arctic. Therefore, we focused on copepods and forage fish during the early life stages with contrasting strong [polar cod and *Calanus* (*Calanus* spp.)] and weaker [saffron cod and *Pseudocalanus* (*Pseudocalanus* spp.)] associations with sea ice as indicators of environmental change on the Chukchi shelf. We assessed variation in (1) spatial distributions of copepods and forage fish among years of differing ice extent to investigate the impacts of sea ice on lower trophic level taxa presence, abundance, and composition, and (2) diet resources ($\delta^{13}C$, $\delta^{15}N$ and CSIAA $\delta^{13}C$) during years with anomalously low sea ice to examine the potential impacts of loss of sea ice and associated shifts in pelagic habitats on basal food web resources. Due to contrasting associations with sea ice habitats, we hypothesize that loss of sea ice alters diet resources and has detrimental impacts on the presence of polar cod and *Calanus*, but has

143 opposing impacts on saffron cod and *Pseudocalanus*, signifying potential changes in Arctic
144 marine food webs and ecosystems.

145 **Methods**

146 ***2.1 Environmental conditions***

147 Physical oceanographic data, ichthyoplankton, and zooplankton were collected in the
148 summer during years of differing sea ice retreat and extent in the Chukchi (lowest: 2011, 2017–
149 2018; intermediate: 2010, 2015; highest: 2012, 2013; Figs. 1 and 2; Supplemental Figs. 1 and 2).
150 The Chukchi is primarily a shallow continental shelf habitat (average depth < 50 m) that extends
151 from Bering Strait in the south to the continental slope of the Arctic Basin in the north (Fig. 1)
152 and is ice covered for ~7 months of the year (Grebmeier et al. 1988).
153

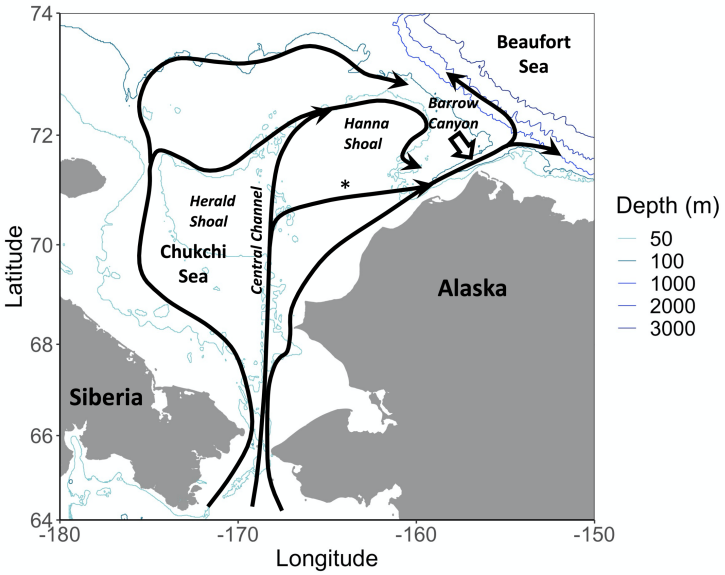

Figure 1. Schematic of prevailing currents (arrows depict major currents), bathymetry contours, mooring location (asterisk), and bathymetric features (italics) in the Chukchi Sea. Adapted from Stabeno et al. (2018) and Corlett and Pickart (2017).

Sea ice extent (km^2) was obtained from the National Snow and Ice Data Center monthly average (https://nsidc.org). Sea ice concentration (percent of grid cell that is covered by ice) was obtained from a NASA Jet Propulsion Laboratory Physical Oceanography Distributed Active Archive Center data product (MUR-JPL-L4-GLOB-v4.1) with a 0.01 degree resolution (grid cell) that includes data from the EUMETSAT Ocean and Sea Ice Satellite Application Facility (OSI SAF) High Latitude Processing Center (https://podaac.jpl.nasa.gov/dataset/MUR-JPL-L4-GLOB-v4.1). As an index of recent sea ice, sea ice concentration was averaged at each grid cell from August 8-September 16 of each year to correspond with the general time period of specimen collections (Supplemental Fig. 2).

Ocean currents can impact water masses and plankton distributions. Therefore, winds from the European Centre for Medium-Range Weather Forecasts ERA5 reanalysis (https://climate.copernicus.eu/climate-reanalysis; Hersbach et al. 2020) and velocity records from moored *in situ* current meters were used to evaluate variability in winds that impact surface currents and depth-averaged currents that reflect motion of the interior water column, respectively. Moorings were equipped with an upward-looking acoustic Doppler current profiler (ADCP; Teledyne RD Instruments) or a single point recording current meter (Aanderaa RCM 9) near the bottom (Stabeno et al., 2018). Data were collected at hourly intervals and processed following manufacturers specifications. Since velocity records typically did not capture the surface boundary layer, depth-averaged currents were calculated. When only a single-point current meter collected data, its values were used because currents are highly correlated in the vertical dimension and little vertical shear exists (Stabeno et al., 2018; Stabeno and McCabe, 2023). Both the winds and currents were low-pass filtered with a cosine-Lanczos window to remove higher frequency variability.

Velocity time series from a single mooring site were chosen and winds from the ERA5 reanalysis were interpolated to this location (Fig. 1). High correlations between currents measured at this site and those measured at other locations throughout the Chukchi suggest this site is representative of typical shelf flows in the region (Stabeno et al., 2018; Stabeno and McCabe, 2023). Wind and current analyses focused on a two-month period (June 15–August 15) to facilitate temporal comparisons among years. Dates generally preceded fish collections (Supplemental Fig. 2) under the assumption that prior events impact dispersal and advection of organisms, and consequently distributions and diet-related isotopic values. Winds and currents were rotated 45° (positive northwest) to match the direction of the coast throughout most of the sampling region (Fig. 1). Strength and directionality of winds impact surface currents and frequent alterations could promote mixing, stirring, and retention. Therefore, the number of along-shelf wind reversals and the decorrelation time scales (calculated as the first zero-crossing of the autocorrelation function) were quantified for each two-month time period.

2.2 Spatial distributions

We focused on polar cod and saffron cod during the early life stages and calanoid copepods (*Calanus* and *Pseudocalanus*) that were primarily collected using a paired 60-cm bongo net (505 μm mesh) coupled with a paired 20-cm bongo net (153 μm mesh) that was towed obliquely from the surface to 10 m off the bottom or a maximum depth of 200 m (Matarese et al., 2003). A Tucker Sled with a 1-m^2 net (333 μm or 500 μm mesh) and a nested 20-cm diameter net (150 μm mesh) towed at a speed to 1.5-2.0 knots was used for some hauls to sample the water column from the bottom to the surface (n = 226 of 598 for fish and n = 50 of 178 for copepods). All nets were equipped with General Oceanics mechanical flowmeters to quantify volume filtered. Samples were preserved in a 5% formalin-seawater solution buffered with

sodium borate and sent to the Plankton Sorting and Identification Center in Szczecin, Poland, for taxonomic identification. Ichthyoplankton were measured to the nearest 0.1 mm standard length (SL). Verification and additional identification to lower taxonomic levels took place at the National Oceanic and Atmospheric Administration's Alaska Fisheries Science Center (NOAA AFSC) in Seattle, WA, USA. Following standardized methods, ichthyoplankton catch per unit effort (CPUE) was calculated as catch per 10 m^2 (Matarese et al., 2003) from 333 μm and 500 μm mesh nets. Fish CPUE was separated into larval (defined as eggs and fish ≤ 30 mm SL) and juvenile (> 30-50 mm SL) age groups (Vestfals et al., 2019), corresponding with age groups used for stable isotope analyses (described below in section *2.3.2*). Copepod CPUE was calculated as catch m^{-3} from 153 μm or 150 μm mesh nets and combined copepodite and adult life stages. *Pseudocalanus* were grouped by genera, and *C. glacialis* and *C. marshallae* were combined following other studies (Hopcroft et al., 2010).

Spatial distribution data were restricted to August 8 to September 15 and latitudes greater than 66 °N to confine surveys to a similar time period and spatial domain (Fig. 2; Supplemental Fig. 2). Distributions of polar cod larvae, polar cod juveniles, *Calanus*, and *Pseudocalanus* in relation to geographic location, sea ice, and sample year were modeled using Generalized Additive Models (GAMs; packages mgcv; R Core Team 2017) to encompass nonlinear relationships between explanatory and response variables (Wood, 2006). Models were not developed for saffron cod due to limited sample sizes (Fig. 2). GAMs addressed differences in spatial and temporal survey design among years (Fig. 2; Supplemental Fig. 2) by including latitude, longitude, and day of year. Models were developed for polar cod using presence/absence data due to a large proportion of zeros (Fig. 2). Logit-linked binomial GAMs rather than zero-inflated modeling approaches (Zuur, 2009) were selected because analyses

223 focused on interannual differences in sea ice and the impacts on polar cod geographic location
224 rather than more subtle differences in abundance among or within years. *Calanus* and
225 *Pseudocalanus* were present at most sampling locations and CPUEs varied by several orders of
226 magnitude, particularly for *Calanus* (Fig. 2), limiting the utility of presence/absence models.
227 Therefore, copepod distributions were modeled with a Tweedie distribution with a log link and
228 power (p; $1 < p < 2$) estimated during model fitting. A Tweedie distribution was selected based
229 on the ability to incorporate positive as well zero catch values (Vestfals et al., 2019; Wood,
230 2006) and comparisons of residuals from Tweedie, negative binomial, and Gaussian distribution
231 models. The most complex model formulations for polar cod larvae and juveniles (eq 1) and
232 *Calanus* and *Pseudocalanu*s (eq 2) were:

233 $$P_j \sim s(LON_j, LAT_j)Year_j + s(DOY_j) + ICE_j + Year_j \quad \text{(eq 1)}$$

234 $$CPUE_j \sim s(LON_j, LAT_j)Year_j + s(DOY_j) + ICE_j + Year_j + \varepsilon_j \quad \text{(eq 2)}$$

235 Where *s* is a smoothing function and *j* is the haul. *P* is presence/absence (separate models for
236 larvae and juveniles), *CPUE* for *Pseudocalanus* is count m^{-3}, and CPUE for *Calanus* is square
237 root transformed count m^{-3} in order to reduce the influence of exceptionally high values. *Year* is
238 collection year, *DOY* is the day of year of sampling, *ICE* is recent sea ice presence or absence at
239 haul locations from gridded satellite data, and ε is the error term. *LAT* and *LON* are incorporated
240 as a two-dimensional smoothing function and include an interaction with *Year* that denotes a
241 separate centered smooth for each year. *Year* is also included as a parametric term that is
242 necessary due to centering constraints (Wood, 2006). GAMs were constructed using thin plate
243 regression spline smooth terms (constrained to 4 knots for one-dimensional terms and 10 for
244 two-dimensional terms; Vestfals et al. 2019). Collinear variables were excluded if variance
245 inflation factors exceeded 3. Models were simplified using backwards elimination, assumptions

were inspected using standard diagnostics (package mgcv, gam.check function; Wood 2006), and model results were plotted (package mgcViz; Fasiolo et al., 2020). Final models were selected based on Akaike Information Criterion (AIC, Akaike 1998) and secondarily based on parsimony as well as Un-Biased Risk Estimator (UBRE), Restricted Maximum Likelihood (REML), or General Cross Validation (GCV) depending on model formulation (binomial, Tweedie, or Gaussian, respectively) if ΔAIC was less than 2.

2.3 Environmental variability and diet resources

During 2017 and 2018, coinciding with unprecedented early ice retreat and low summer sea ice (Supplemental Fig. 1), a targeted study with expanded physical oceanographic data was conducted to determine the impacts of environmental conditions on diet-related stable isotopes and carbon sources of focal taxa. Measurements from shipboard conductivity, temperature, depth recorders (CTD; temperature, salinity, and fluorescence) were obtained from vertical profiles at each station taken either immediately before or following plankton collections. Data were collected using a Sea-Bird Electronics (SBE) 911*plus* system equipped a WET Labs ECO-AFL/FL fluorescence sensor, processed using SBE software, and averaged in 1 m depth bins.

Water samples were used to calibrate conductivity measurements and to correct fluorescence (flu) measurements. Discrete chlorophyll-*a* (chl-*a*) samples, available from a subset of stations, were filtered through Osmonics glass fiber filters, stored at -80°C, and analyzed within 6 months of collection. Chl-*a* was extracted in 90% acetone for 24 hours and concentrations were determined using the acidification method (Lorenzen 1966) with a Turner Designed TD700 fluorometer calibrated with pure chl-*a* or a Turner Designed Trilogy with a chl-*a* acidification module. For each survey, flu and chl-*a* for the corresponding cast and depth bin (1 m) were used to develop linear correction equations (OS17-01: chl-*a* =0.65*flu+0.43, $p<0.0001$,

r^2=0.42, $F_{1,457}$=330.7; HE17-02: chl-*a* =2.67*flu-0.43, p<0.0001, r^2=0.75, $F_{1,343}$=1032; HE18-01: chl-*a* =0.27*flu-0.21, p<0.0001, r^2=0.44, $F_{1,459}$=357.4). Note that OS17-01, HE17-02, and HE18-01 are referred to respectively as surveys 2017a, 2017b, 2018 in the manuscript to differentiate years. Following flu corrections, values are reported as chl-*a* (mg m^{-3}) for analyses.

Pelagic environments on the Chukchi shelf are strongly influenced by water masses that can be categorized to a certain extent from temperature and salinity (Corlett and Pickart 2017; Danielson et al., 2017). These designations reflect water origin and a suite of conditions and organisms associated with particular water masses (Logerwell et al., 2020; Spear et al., 2019). Therefore, water masses were defined throughout the water column using temperature and salinity data from CTD casts to depths of 200 m, corresponding with net tows and the estimated depth range of young polar cod (Bouchard et al. 2016). Designations generally followed guidelines from Corlett and Pickart (2017), but were reduced to four categories in order to focus on water masses linked with sea ice and warm waters that enter the Chukchi through Bering Strait. Reduced categories were determined from similarities in water mass origin, temperature and salinity (Fig. 3a showing continuity between groups), and depth profiles (Fig. 3b, c). Following inspection of temperature and salinity biplots and depth profiles, *Melt* water and *Atlantic* water were retained, but *Alaskan coastal* and *Bering summer* waters were combined to designate *Pacific* water, and *Remnant winter* and *Newly ventilated winter* waters were combined and designated as *Cold shelf* (Fig. 3). We note that water mass designations from temperature and salinity alone provide guidelines, but are unable to unambiguously separate low salinity surface waters derived from runoff from melted sea ice in the absence of additional data such as nutrients or stable isotopes (Mueter et al. 2021). However, there is a precedent for applying water

291 mass designations from temperature and salinity in the Chukchi, and guidelines are similar
292 among studies (Corlett and Pickart 2017; Danielson et al., 2017).

293 Bulk stable isotopes ($\delta^{13}C$ and $\delta^{15}N$) and CSIAA $\delta^{13}C$ included specimens collected
294 throughout the duration of each survey to obtain sufficient sample sizes (August 11-September
295 12, 2017 and August 11-August 23, 2018). *Calanus* and *Pseudocalanus* (adult stages only, due to
296 challenges identifying frozen samples), polar cod larvae and juveniles (≤ 37 mm), and saffron
297 cod (≤ 29.5 mm) from 153 μm and 500 μm mesh nets were frozen at -80°C. *Calanus glacialis*
298 comprised the majority of identifiable *Calanus* species from frozen samples used for this study
299 (E. D. Goldstein, *personal observation*).

300 For zooplankton bulk isotope analyses, whole specimens were dried at 50°C until a stable
301 weight was maintained. Samples were then homogenized and prepared in tin capsules. Copepods
302 that were co-collected (same haul) were composited in a single capsule to obtain sufficient
303 sample weight.

304 CSIAA requires more tissue than bulk analyses, and was therefore limited to only fish.
305 Bulk analyses were performed for fish if tissue was available after CSIAA or if the total sample
306 weight was not sufficient for CSIAA. Heads and stomachs were removed and the remaining
307 tissue was dried at 50°C or freeze dried. If necessary, samples from the same haul were
308 combined to obtain sufficient weight within a size range of ± 3 mm (< 2 SD) from the mean SL
309 of the fish used for the composite. For composites, mean SL was used for analyses.

310 All stable isotope analyses were conducted at NOAA AFSC in Juneau, Alaska, USA.
311 Tissues for bulk analyses were analyzed using a Thermo Scientific FlashSmart elemental
312 analyzer in line with a ThermoFinnigan DeltaPlus XP continuous-flow isotope ratio mass
313 spectrometer (CF-IRMS; Thermo Scientific, Bremen, Germany). Measured $\delta^{13}C$ and $\delta^{15}N$ values

obtained from bulk isotopic sample analysis were scale-calibrated on the basis of contemporaneously analyzed isotope reference materials of accepted δ values relative to the appropriate reference scale acting as scale anchors. Relative stable isotope abundance values are reported in δ notation and are given as per mil values (‰). The isotope reference materials used were supplied by the International Atomic Energy Agency (IAEA-N-1, $\delta^{15}N = 0.4 \pm 0.2$ ‰; IAEA-CH-7, $\delta^{13}C = -32.151 \pm 0.050$ ‰; IAEA-CH-3, $\delta^{13}C = -24.724 \pm 0.041$ ‰) and the United States Geological Survey (USGS25, $\delta^{13}C = -34.58 \pm 0.06$ ‰, $\delta^{15}N = -0.94 \pm 0.16$ ‰; USGS40, $\delta^{13}C = -26.389 \pm 0.042$ ‰, $\delta^{15}N = -4.5 \pm 0.1$ ‰; USGS41, $\delta^{13}C = +37.626 \pm 0.049$ ‰, $\delta^{15}N = 47.6 \pm 0.2$ ‰). Internal laboratory standards were included with all samples as quality controls. Internal laboratory standards had the following values and error (SD): purified methionine, Alfa Aesar, $\delta^{13}C = -34.58 \pm 0.06$ ‰, $\delta^{15}N = -0.94 \pm 0.16$ ‰; homogenized Chinook salmon muscle, NOAA Fisheries, $\delta^{13}C = -19.27 \pm 0.05$ ‰, $\delta^{15}N = 15.56 \pm 0.13$ ‰). Long-term records of internal standards yield an analytical precision (standard deviation) of 0.11 and 0.12‰ for $\delta^{13}C$ and for $\delta^{15}N$, respectively.

Lipids are depleted in ^{13}C compared to other tissues (Post et al., 2007), so bulk $\delta^{13}C$ values were corrected following Marsh et al. (2017) using equation (eq 3) for fish (Post et al., 2007) and equation (eq 4) for copepods (El-Sabaawi et al., 2009):

$$\delta^{13}C_{cor} = \delta^{13}C_{measured} - 3.32 + 0.99 * C{:}N \quad \text{(eq 3)}$$

$$\delta^{13}C_{cor} = \delta^{13}C_{measured} - 1.85 + 0.38 * C{:}N \quad \text{(eq 4)}$$

where $\delta^{13}C_{cor}$ (henceforth referred to as $\delta^{13}C$) is the lipid-corrected value, $\delta^{13}C_{measured}$ is the measured value from bulk isotope analyses, and C:N is the carbon to nitrogen ratio for each sample.

CSIAA sample preparation utilized a chloroformate-based method for amino-acid derivatization (Walsh et al., 2014) and analysis was performed using a Trace 1310 gas chromatograph (Thermo Electron, Bremen Germany) on a DB-23 column (Agilent Technologies) coupled to a Delta V Advantage isotope ratio mass spectrometer via an Isolink II combustion interface (Thermo Electron, Bremen, Germany). For amino acid $\delta^{13}C$ analysis, a 10 mg sample of freeze-dried and homogenized tissue was acid-hydrolyzed in a 6M HCl solution for 70 min and then dried down in a temperature-controlled heating block at 60 °C under a stream of purified nitrogen gas. The hydrolyzed amino acids were then derivatized in a solution of methanol, pyridine, and methyl chloroformate (Sigma Aldrich, St. Louis, MO, USA) using a one-step rapid derivatization method (Walsh et al., 2014) which has proven to be a simple, rapid, and reliable method for $\delta^{13}C$ studies (Ohkouchi et al., 2017). Compound-specific ^{13}C amino acid analysis was performed using a Trace 1310 gas chromatograph (Thermo Electron, Bremen Germany) on a DB-23 column (Agilent Technologies). The gas chromatograph was coupled to a Delta V Advantage isotope ratio mass spectrometer via an Isolink II combustion interface (Thermo Electron, Bremen, Germany) at a reactor temperature of 1000 °C. For each analysis, a 0.5 µl aliquot of derivatized sample was injected into a deactivated splitless liner (Restek Corporation, Bellefonte, PA) at 250 °C with a helium flow rate of 1.2 ml/ min. For each sample, the $^{13}C/^{12}C$ ratio was determined and calibrated to the international reference standard scale, Vienna Pee Dee Belemnite (VPDB). Each sample was arithmetically corrected for the addition of carbon during derivatization by running purified and derivatized amino acids of a known isotopic value throughout the analytical sequence and applying a correction factor according to the method described by Docherty et al. (2001).

2.3.1 Isotopic niche

Three complementary methods were employed to determine isotopic niche, indicative of the breadth of diet resources, based on variability in bulk $\delta^{13}C$ and $\delta^{15}N$ in biplot space: convex hulls, standard ellipses using Maximum Likelihood with a correction for small sample size (SEA_C), and standard ellipses using a Bayesian framework (SEA_B) to account for bias due to sample sizes and unbalanced datasets (package SIBER; R Core Team 2017; Jackson et al. 2011). Analyses excluded some samples to obtain comparable within-species spatial coverage between years. Area of the truncated sample regions (excluding land) were calculated to compare with SEA_B.

2.3.2 Environmental influences on basal carbon sources

Factors that influence basal carbon sources for fish were determined using $\delta^{13}C$ of essential AA [Isoleucine (Iso), Lysine (Lys), Leucine (Leu), Methionine (Met), Phenylalanine (Phe), and Valine (Val)]. Data were visualized with Principal Component Analyses (PCA) for each species (excluding Met that was not measured for all specimens). PCA axis 1 scores were then utilized as response variables in GAMs to assess the influence of the environment on diet resources.

The water column in the Chukchi is depth-structured (Danielson et al. 2017) and young fish or their prey could access carbon sources across depths (Bouchard et al. 2016; Runge and Ingram, 1991). Therefore, GAMs, modeled with a Gaussian distribution, were used to address the influences of the local physical environment and chl-*a* on CSIAA $\delta^{13}C$ of polar cod (due to limited sample sizes of saffron cod). Physical variables throughout the top 200 m of the water column were averaged because the depths of the fish were unknown, and while polar cod are typically in the top 40 m of the water column, they can access resources at greater depths (Bouchard et al., 2016). Additionally, initial data exploration partitioning the water column

according to pycnocline depth (calculated for each station from CTD data) yielded negligible depth-specific relationships with CSIAA $\delta^{13}C$ and the physical environment, despite the expectation that the pycnocline acts as a boundary or region of aggregation for fish larvae (Houde 2016). Therefore, the first model formulation incorporated depth-averaged environmental variables:

$$PC_{i,j} \sim s(SL_{i,j})Year_j + s(S_j)Year_j + s(T_j)Year_j + s(C_j)Year_j + Year_j + \varepsilon_{i,j} \quad (5)$$

where s is a one-dimensional smoothing function, i is sample (individual fish tissue or composite) and j is the haul. PC is the PCA axis 1 score, SL is fish standard length (or average length for composite samples), S is average salinity, T is average temperature, C is average chl-*a*, and ε is the error term. Interactions between smooth terms and the factor *Year* denote the inclusion of a separate centered smooth for each year (2017 and 2018). *Year* is a fixed effect in the model that adds or subtracts a constant from the smoother for each year and is necessary due to centering constraints (Wood 2006).

The second model formulation addressed whether carbon sources reflect changes in water masses, as indicators of pelagic ecosystem shifts. Specifically, we explore whether the influx of *Pacific* water or designations of sea ice signatures (*Melt*) impacted CSIAA. Not all water masses were present at all stations, constraining factor level designations. Therefore, stations at which *Melt* water was present in the water column were deemed *Melt* influenced as an indicator of sea ice-influenced habitats. If *Melt* water was not present, but *Pacific* water was, then the station was categorized as *Pacific* influenced. Fish size was included as a covariate because prey may differ throughout growth and ontogeny. Chl-*a* was included to address the potential relationship between primary producers and ^{13}C enrichment due to blooms (de la Vega et al., 2019). The most complex model formulation was:

$$PC_{i,j} \sim s(SL_{i,j})Year_j + s(C_j)WM_j + WM_j + Year_j + \varepsilon_{i,j} \quad (6)$$

Following the same notation described for equation 5 with the exception of *WM* that refers to *Melt* influenced or *Pacific* influenced locations (hauls) and was included as a factor. Both equations (5) and (6) followed the same model selection procedures described for equations (1) and (2).

2.3.3 Basal carbon source contributions

Carbon source contributions were assessed using isotope "fingerprints" from $\delta^{13}C$ of essential AA from the forage fish and published values from the literature for potential sources (Supplemental Table 1). "Fingerprints" are patterns in $\delta^{13}C$ that differ among primary producers and can be used to identify carbon sources regardless of sample origin (Larsen et al., 2013; Rowe et al., 2019, Whiteman et al., 2019). To obtain "fingerprints", mean essential AA $\delta^{13}C$ was calculated (i.e. average across Ile, Val, Phe, and Leu due to data availability; Supplemental Table 1) and then subtracted from each unique $\delta^{13}C$ essential AA value (e.g. mean centered) for each sample (Larsen et al., 2013). "Fingerprints" of Arctic gadids coincide with the primary producers consumed by their major diet sources (copepod nauplii, copepodites, and some later copepod stages; Bouchard and Fortier, 2020). Potential carbon source "fingerprints" were initially incorporated a higher taxonomic resolution for microalgae than other groups due to its importance in copepod diets (El-Sabaawi et al., 2009; Levinsen et al., 2000; Vargas and González, 2004) and to differentiate between diatom-dominated sea ice algae (von Quillfeldt et al., 2003) and pelagic phytoplankton.

PCA and Linear Discriminant Analysis (LDA) were used to assess similarities between "fingerprints" from potential carbon sources, polar cod larvae and juveniles, and saffron cod (combined age groups for analyses due to sample sizes) and to inform source categories for

isotope mixing models. The LDA (package MASS; R Core Team 2017) focused on taxonomic categories and therefore excluded coarse groupings [sea ice particular organic matter (iPOM), pelagic particular organic matter (pPOM), seston, and fjord], as well as macroalgae that are likely not consumed by copepods. Phe was also excluded because it was collinear with Val, violating an assumption of the analysis. Following initial formulation, taxa were iteratively grouped according to proximity in multivariate space in PCAs and LDAs until correct LDA predictions with leave-one-out cross validation were greater than 50% for all groups. This resulted in three carbon source groups: (1) Microalgae (cryptophytes, chrysophytes, some genera of cyanobacteria, haptophytes, chlorophytes, and diatoms); (2) Syn + Dino [*Synechococcoccus* and dinoflagellates; *Synechococcoccus* ordinated more closely with dinoflagellates than other cyanobacteria and were present in the Chukchi in recent years (Lomas et al., 2021)]; and (3) Bacteria. LDAs were then used to predict carbon source group membership (projections onto linear discriminants) of iPOM and pPOM to make inferences about their taxonomic composition, and to inform the potential inclusion of the two groups in the mixing models. LDA predictions of gadid "fingerprints" were used to determine likely diet resources.

Following the LDA that focused on taxonomic-groupings, Bayesian stable isotope mixing models (MixSIAR; R core team 2017; Stock and Semmens, 2018) were employed to assess the relative contributions of iPOM, pPOM, and Syn + Dino to fish diets. Multivariate analyses indicated that iPOM and pPOM were primarily comprised of microalgae, but were dissimilar to *Synechococcoccus* and dinoflagellates, suggesting that the three groups reflect sea ice, pelagic, and potentially subarctic (Flombaum et al., 2013) habitats and food sources. Fish "fingerprints" were also dissimilar to Bacteria (Supplemental Fig. 3). Therefore, an *a priori* approach (Phillips et al., 2014) with three end-members (iPOM, pPOM, and Syn + Dino) and

four isotope tracers (Ile, Leu, Val, as well as Phe) was used for mixing models. Separate models were developed for each fish species using a nominal trophic discrimination factor of 0.1 ± 0.1‰ (McMahon et al., 2010). Models included a multiplicative error term to account for residual error and process error (Stock and Semmens, 2016). Factors were included as combinations of age groups and years for polar cod, and only year for saffron cod, due to small sample sizes that prohibited other model formulations. Factor levels are biologically related, and were therefore included as random effects which allowed the model to "borrow strength" between groups by using a shared distribution with factor level offsets (Stock et al. 2018). Models were run with 1,000,000 iterations, with a burn-in of 500,000, a thinning factor of 500, and 3 chains to reach model convergence based on Gelman-Rubin diagnostic and the Geweke diagnostic (Stock and Semmens, 2018).

2. Results

3.1 Environmental conditions

Summer sea ice during the study was lower than most years in recent decades, with the earliest ice retreat in 2017 and 2018, and the lowest extent from late spring through early fall (May-August) since 1979 during 2017 (Supplemental Fig. 1). Within the survey region, summer sea ice concentration was greatest in 2012 and 2013, followed by 2015 when ice was primarily off the shelf (Fig. 2).

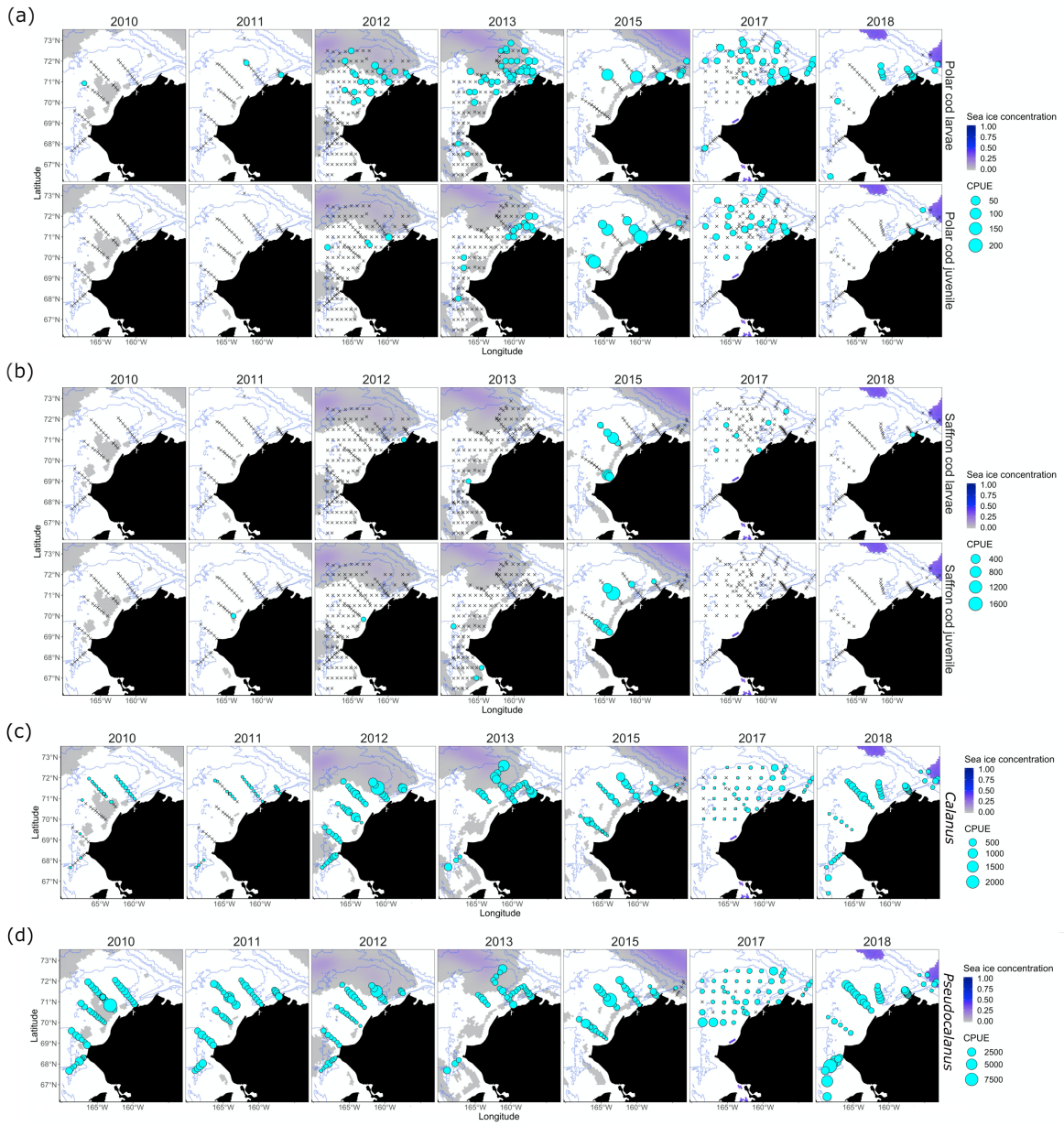

Figure 2. Polar cod (a), saffron cod (b), *Calanus* (c) and *Pseudocalanus* (d) CPUE (count per 10 m^2 for fish and count m^{-3} for copepods). Larvae are eggs and fish ≤30 mm standard length (SL) and juveniles are >30-50 mm SL. Sea ice concentration (color field) is averaged from August 8 to September 15 in each year. Stations with zero catch are shown as an "x".

469

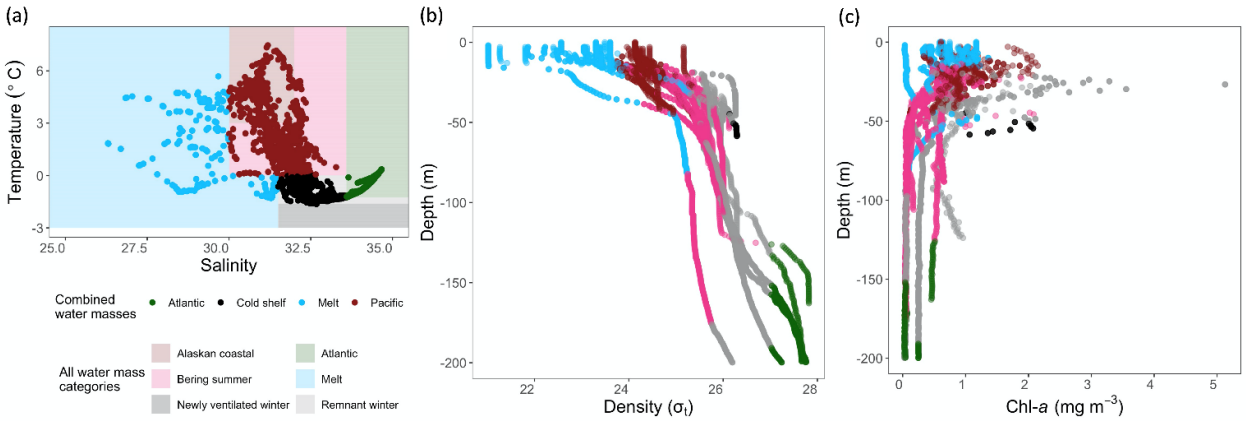

Figure 3. Temperature, salinity, density, and chl-*a* from CTD casts from 2017 and 2018 that coincided with fish collections for stable isotope analyses. In (a), "All water mass categories" are designations from Corlett and Pickart (2017) and are shown as rectangle polygons. "Combined water masses" are shown as points. Data were collected throughout the water column at each station and points are temperature and salinity measurements from CTD casts. Density and chl-*a* profiles in (b) and (c) are color coded by "All water mass categories" and show depth profiles from CTD measurements taken at the same stations as (a).

The frequency of along-shelf wind reversals and the magnitude of winds differed among years, but there were often periods of a week or greater with a relatively sustained wind direction (Fig. 4a). Winds were southwestward immediately prior to and up until specimen collections for all years excluding 2012 and 2017. Over the two month period, winds in 2017 were distinctive from other years as having the lowest decorrelation time scale and highest number of reversals. Decorrelation timescales were also low in 2011, but the number of reversals was reduced compared to 2017 (Fig. 4a).

Along-shelf currents were primarily northeastward in agreement with prevailing currents (Figs. 1 and 4b). Currents flowed to the southwest more frequently during the years with early ice retreat and low sea ice coverage (2017 and 2018). The lowest mean northeastward current velocity was in 2017, and 2018 was the only year with a southwestward mean current. During 2017, southwestward currents were primarily during the sampling time period, but in 2018 they were prior to and during collections.

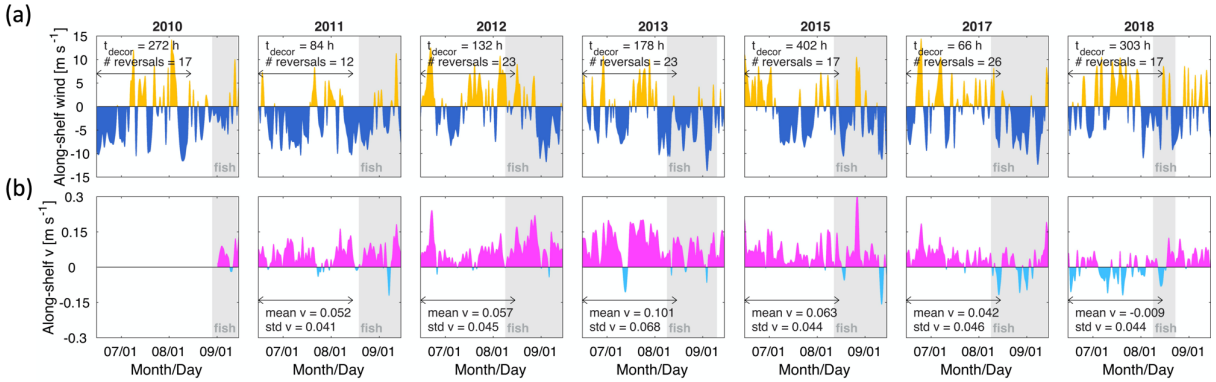

Figure 4. (a) Time series of ERA5 along-shelf winds, and (b) depth-averaged along-shelf currents at a mooring site in the Chukchi (see Fig. 1). Winds and currents were rotated 45 degrees, with positive values toward the northeast. Gray shading denotes periods of larval fish and copepod collections. Decorrelation time scales and the number of along-shelf wind reversals during a two-month period (arrows; Jun 15 to Aug 15) are indicated in the top panels. The means and standard deviations of the depth-averaged along-shelf currents over the same time period (arrows) are provided in the lower panels.

3.2 Spatial distributions

GAMs indicated that polar cod occurrence was related to geographic location and sea ice, but low deviance explained suggested that additional factors also impact distributions (Table 1). Polar cod larvae and juveniles occurred most frequently in the northern regions of the study domain; particularly to the southeast of Hanna Shoal and near Barrow Canyon. However,

distributions differed among years and between life stages (Fig. 2a, Supplemental Figs. 4 and 5). Larval occurrence was not influenced by sea ice or DOY. Juvenile occurrence had a weak positive relationship with DOY and was impacted by sea ice as evidenced by juvenile presence in open water rather than overlapping with sea ice, particularly near the coast during 2012 and 2013 (Table 1, Fig. 2a, Supplemental Fig 5). Model results in 2010 and 2011, however, were spurious and confirm the influence of other processes on distributions (Fig. 2a, Supplemental Fig. 5). During 2017, when sea ice was exceptionally low, presence/absence of polar cod juveniles was more uniform along the east-west direction than other years (Fig. 2a, Supplemental Fig. 5). During 2018, the other year with extremely early ice retreat (Supplemental Fig. 1), variation in occurrence of larval and juvenile polar cod was greatest in the east-west direction, and juveniles were rare but concentrated in the northeast (Fig. 2a; Supplemental Figs. 4 and 5).

Saffron cod were rare in most years, limiting conclusive findings. Larvae and juveniles were only found in open water, rather than regions with recent sea ice, and catches were highest during 2015. Larvae, but not juveniles, were also present in 2017. Limited presence in other years was nearshore and at lower latitudes (Fig. 2b).

Calanus distributions had some similarities with polar cod such as generally higher concentrations at higher latitudes and in the northeastern region near Barrow Canyon and south of Hanna Shoal (Fig. 2, Supplemental Figs. 4-6). In addition to year and geographic location, the final model for *Calanus* included a weak inverse relationship between CPUE and DOY (reduced abundance later in the summer) and a positive relationship with recent sea ice (Table 1, Supplemental Fig. 6). *Calanus* were more abundant during years of greater ice extent (2012–2015) compared to years with lower summer sea ice with the exclusion of 2018 (Supplemental Fig. 6).

513 *Pseudocalanus* were ubiquitous and CPUE was not influenced by sea ice or DOY.
514 Distributions differed among years but lacked consistent geographic patterns (Table 1, Fig 2d,
515 Supplemental Fig. 7). *Pseudocalanus* abundance varied between years but was discordant with
516 sea ice extent or presence. For example, CPUE was low from 2012–2017, encompassing years
517 when sea ice extent varied substantially (Table 1, Fig 2d, Supplemental Fig. 7).
518
519 **Table 1.** Generalized Additive Models showing the top two models (final model in bold with
520 asterisk) for polar cod larvae, polar cod juveniles, *Calanus*, and *Pseudocalanus* spatial
521 distributions as well as models addressing relationships between water mass and $\delta^{13}C$ CSIAA of
522 polar cod. Model equations (eq) and variables are described in the methods, but are simplified here
523 to exclude subscripts and error terms. Detailed model results are provided for the final model with
524 the exception of water mass models where the top two models had similar AIC and substantial
525 differences in deviance explained (Dev. expl.), but the final model was selected based on
526 parsimony and GCV (0.02 for both). Smooth term p-values and effective degrees of freedom (edf)
527 are shown as well as p-values and term estimates (estimate) for parametric terms.
528

Model description	Best-fit models	Dev. expl.	AIC	Smooth term: p-value (edf)	Parametric term: p-value (estimate)
(eq 1) Polar cod larvae distributions n_{total} = 621	***P ~ s(LON, LAT)Year + Year**	**29.5**	**489.91**	***(LON,LAT)*$_{2010}$: 0.86 (2.81)** ***(LON,LAT)*$_{2011}$: 0.38 (2.00)** ***(LON,LAT)*$_{2012}$: 0.10 (4.33)** ***(LON,LAT)*$_{2013}$: <0.001 (2.00)** ***(LON,LAT)*$_{2015}$: 0.03 (2.00)** ***(LON,LAT)*$_{2017}$: 0.03 (2.23)** ***(LON,LAT)*$_{2018}$: 0.84 (8.77)**	**Intercept: 0.71 (-84.32)** ***2011*: 0.73 (79.02)** ***2012*: 0.72 (81.69)** ***2013*: 0.72 (83.27)** ***2015*: 0.72 (80.99)** ***2017*: 0.72 (82.78)** ***2018*: 0.76 (70.01)**
	P ~ s(LON, LAT)Year + s(DOY) + Year	29.8	490.23	-	-
(eq 1) Polar cod juvenile distributions n_{total} = 621	***P ~ s(LON, LAT)Year + DOY + ICE + Year**	**32.4**	**309.48**	***(LON,LAT)*$_{2010}$: 1.00 (2.00)** ***(LON,LAT)*$_{2011}$: 1.00 (2.00)** ***(LON,LAT)*$_{2012}$: 0.38 (2.00)** ***(LON,LAT)*$_{2013}$: 0.39 (7.37)** ***(LON,LAT)*$_{2015}$: 0.20 (2.00)** ***(LON,LAT)*$_{2017}$: 0.21 (2.00)**	**Intercept: 1.00 (-92.55)** ***DOY*: 0.02 (0.07)** ***ICE*: 0.08 (1.18)** ***2011*: 1.00 (-2.89)** ***2012*: 1.00 (71.30)** ***2013*: 1.00 (70.65)**

				***(LON,LAT)*$_{2018}$: 0.99 (2.81)**	***2015*: 1.00 (73.25)** ***2017*: 1.00 (72.31)** ***2018*: 1.00 (-1227.00)**
	P ~ s(LON, LAT) + DOY + ICE + Year	22.0	315.91	-	-
(eq 2) *Calanus* distributions n_{total} = 331	***CPUE ~ s(LON, LAT)Year + s(DOY) + ICE + Year***	**75.6**	**1624.74**	***(LON,LAT)*$_{2010}$: <0.001 (4.20)** ***(LON,LAT)*$_{2011}$: 0.002 (5.48)** ***(LON,LAT)*$_{2012}$: 0.07 (2.00)** ***(LON,LAT)*$_{2013}$: 0.14 (2.00)** ***(LON,LAT)*$_{2015}$: <0.001 (7.99)** ***(LON,LAT)*$_{2017}$: <0.001 (4.86)** ***(LON,LAT)*$_{2018}$: 0.003 (6.62)** ***(DOY)* : 0.24 (1.93)**	**Intercept: 0.05 (0.87)** ***ICE*: 0.02 (-0.28)** ***2011*: 0.05 (-1.06)** ***2012*: <0.001 (2.01)** ***2013*: <0.001 (1.94)** ***2015*: 0.09 (0.97)** ***2017*: 0.81 (0.12)** ***2018*: <0.001 (1.64)**
	CPUE ~ s(LON, LAT)Year + ICE + Year	75.3	1625.47	-	-
(eq 2) *Pseudocalanus* distributions n_{total} = 331	***CPUE ~ s(LON, LAT)Year + Year***	**49.8**	**4970.71**	***(LON,LAT)*$_{2010}$: 0.70 (4.56)** ***(LON,LAT)*$_{2011}$: 0.70 (2.00)** ***(LON,LAT)*$_{2012}$: <0.001 (5.85)** ***(LON,LAT)*$_{2013}$: 0.85 (2.00)** ***(LON,LAT)*$_{2015}$: <0.001 (7.03)** ***(LON,LAT)*$_{2017}$: <0.001 (6.98)** ***(LON,LAT)*$_{2018}$: <0.001 (6.51)**	**Intercept: <0.001 (6.84)** ***2011*: 0.49 (0.20)** ***2012*: 0.31 (-0.33)** ***2013*: 0.52 (-0.20)** ***2015*: 0.29 (-0.37)** ***2017*: 0.09 (-0.58)** ***2018*: 0.11 (0.46)**
	CPUE ~ s(LON, LAT)Year + ICE + Year	49.7	4970.38		
(eq 5) Local physical environment n_{total} = 37	***PC ~ SL + C* linear model: R^2_{adj} = 0.13**	-	**-27.80**	-	**Intercept: 0.70 (0.05)** **SL: 0.13 (-0.01)** **C: 0.03 (0.16)** **Model: 0.04**
	PC ~ *s*(*SL*) + *s* (*C*)	17.7	-27.80	*SL*: 0.13 (1.0) *C*: 0.03 (1.0)	Intercept: 1.00 (0.00)
(eq 6) Water masses n_{total} = 36	***PC ~ s(C)WM + WM***	**43.8**	**-34.32**	***C*$_{\text{Pacific influence}}$: 0.02 (1.00)** ***C*$_{\text{Melt influence}}$: 0.005 (2.90)**	**Intercept: 0.81 (0.01)** ***Pacific influence*: 0.34 (-0.05)**
	PC ~ s(C)WM + WM + Year	47.6	-34.81	$C_{Pacific\ influence}$: 0.01 (1.00) $C_{Melt\ influence}$: 0.01 (2.91)	Intercept: 0.51 (-0.02) *Pacific influence*: 0.47 (-0.03) *2018*: 0.17 (0.08)

3.2 Isotopic niche

Spatial patterns in bulk $\delta^{13}C$ were more uniform during 2017 than 2018 for all taxa (Fig. 5a). During 2018, $\delta^{13}C$ of copepods and polar cod increased inshore to offshore along the tightly-packed stations across Barrow Canyon (Fig. 1; Fig. 5a). Copepod collections covered a large geographic area and indicated that ^{13}C was depleted off the slope north of Barrow Canyon (dark grey for *Calanus* and color scale for *Pseudocalanus*; Fig. 5a, b) and ^{15}N was depleted in the south compared to north (light vs. dark gray; Fig. 5).

Polar cod collection locations covered a greater spatial domain in 2017 than 2018, but isotopic niche was reduced. This was primarily due to a narrower range of $\delta^{13}C$ (Fig 5; Table 2). Reduced breadth of $\delta^{13}C$ was also evident for *Calanus* despite similar isotopic niche estimates between years for the copepod (Fig 5; Table 2). *Pseudocalanus* isotopic niche was similar for both years (Table 2). Sample size of saffron cod was low in 2017, but isotopic niche during 2018 was influenced by $\delta^{15}N$ to a greater degree than $\delta^{13}C$ (Fig. 5b).

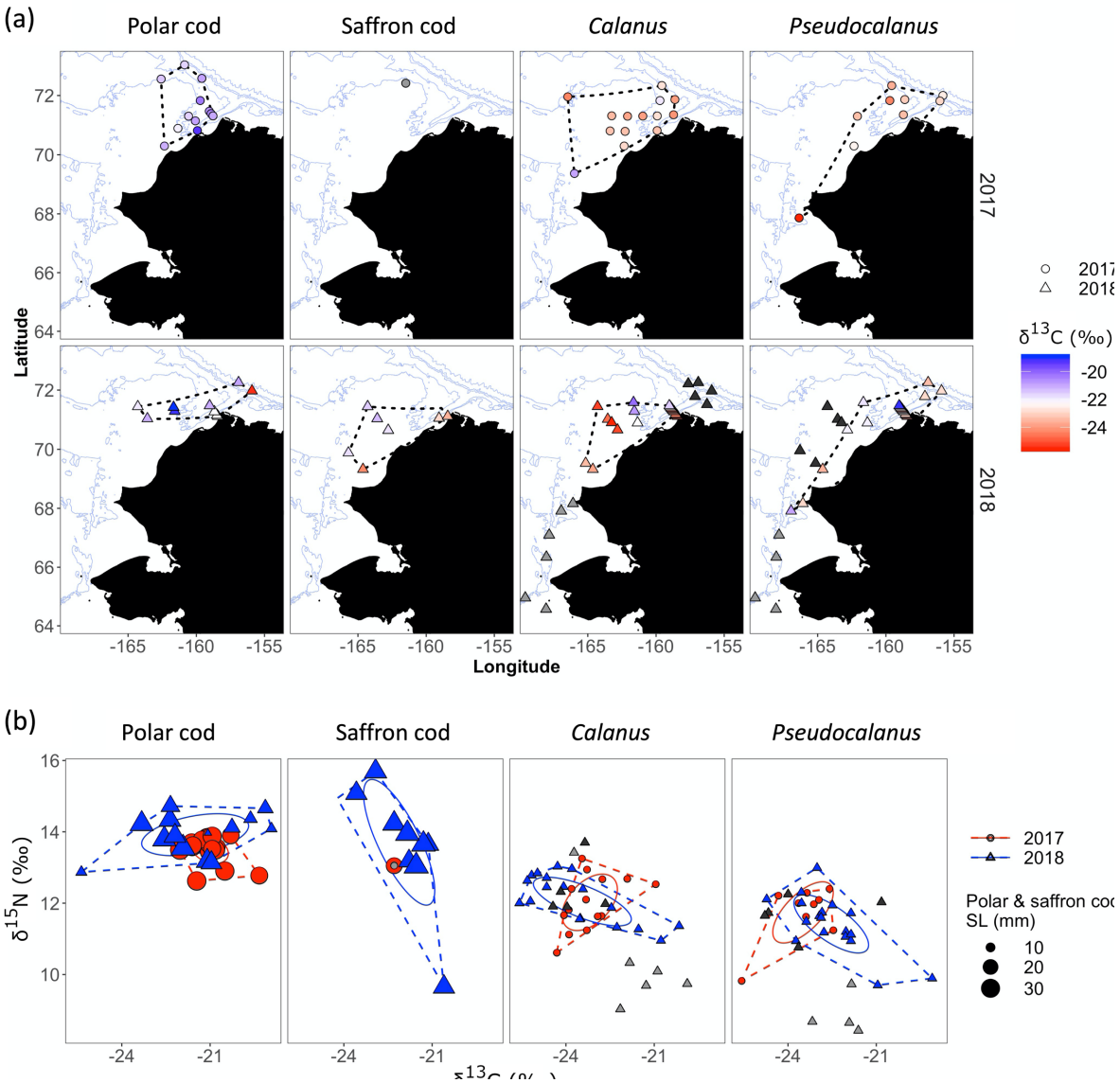

Figure 5. (a) Bulk stable isotope collection locations. Points (specimens) within polygons (dotted lines) were used in isotopic niche calculations and gray symbols (light gray for points south of polygons and dark gray for all others) were excluded (Table 2). (b) Bulk stable isotopes biplots. Colors show collection year and gray symbols correspond to those outside of the polygons in (a). Dotted lines are isotopic niche estimates from convex hulls and solid lines are 95 % prediction ellipses (SEAc; see Table 2).

543

Table 2. Isotopic niche estimates from bulk $\delta^{13}C$ and $\delta^{15}N$ stable isotope values (see Fig. 5). Ellipse areas were calculated using maximum likelihood with a correction for small sample size (SEAc) and a Bayesian approach (SEA_B). SEA_B standardized to spatial area was calculated by dividing SEA_B and credible intervals by spatial area for each taxon and year.

Taxa	Year	Spatial area (km^2)	Convex hull area	Ellipse area (SEAc/SEA_B)	SEA_B 95% credible interval (CI) (low, high)	SEA_B (CI low, CI high) standardized to spatial area $‰^2\ km^{-2} * 10^{-5}$
Polar cod	2017	38495	2.28	0.76/0.76	0.41, 1.13	1.97 (1.07, 2.94)
Polar cod	2018	29717	7.04	3.05/3.09	1.60, 4.82	10.40 (5.38, 16.22)
Saffron cod	2017	na	na	-	-	-
Saffron cod	2018	46422	7.84	4.32/4.52	1.91, 7.66	9.74 (4.11,16.50)
Calanus	2017	78996	3.77	2.07/2.09	1.07, 3.30	2.65 (1.35, 4.18)
Calanus	2018	44133	5.08	2.48/2.62	1.38, 4.00	5.94 (3.13, 9.06)
Pseudocalanus	2017	57974	3.85	2.11/2.24	0.90, 3.87	3.86 (1.55, 6.68)
Pseudocalanus	2018	57126	7.97	2.26/2.31	1.29, 3.45	4.04 (2.26, 6.04)

3.3 Basal carbon sources

Essential AA were generally ^{13}C-depleted compared to non-essential AA in accordance with minimal enrichment from trophic fractionation (Fig. 6a). There was variability in $\delta^{13}C$ among essential AA (particularly Iso and Lys compare to the others) following expectations for isotopic "fingerprinting" methods that rely on essential AA isotopic variation (Larsen et al. 2009). Polar cod and saffron cod had similar essential AA $\delta^{13}C$ values, but during 2018 when some saffron cod were also caught farther south (Fig. 7), there was a slight divergence between species.

Concurrent enrichment or depletion of ^{13}C of all five essential AA coincided with the majority of the variability in the data. The first two Principal Component (PC) axes did not reflect changes in SL, but PC2 diverged between years. For both species, PC2 was most strongly related to ^{13}C-enriched Lys and Val during 2018 and Phe during 2017 (Fig. 6b, c).

561

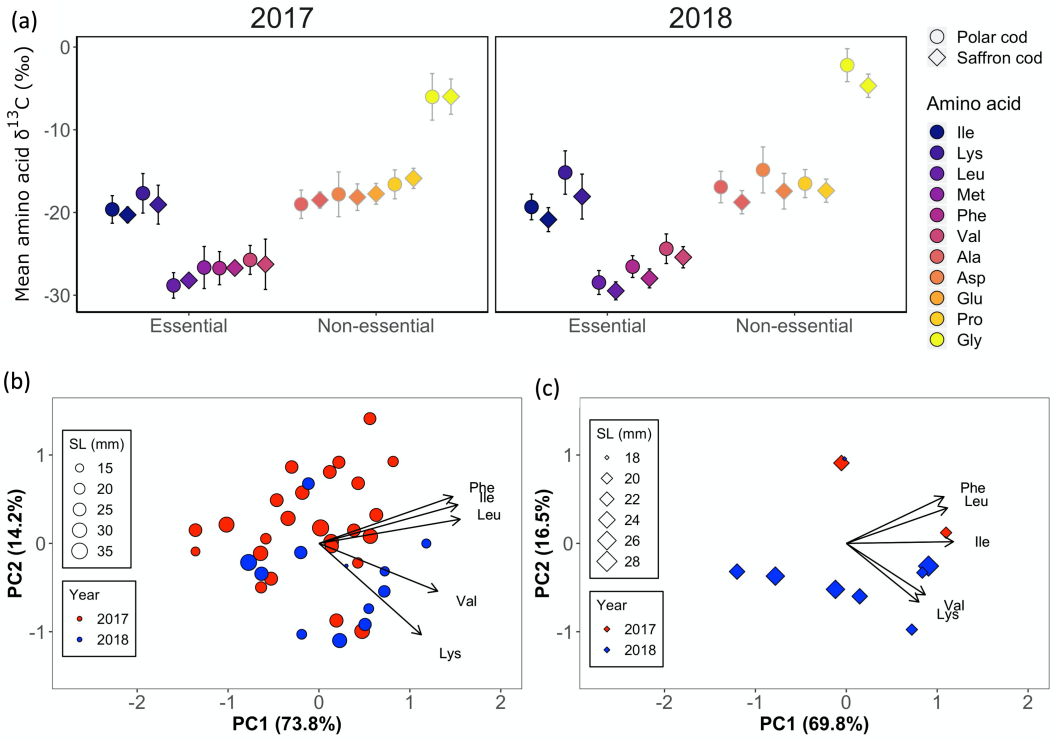

Figure 6. (a) Mean (±SD) $\delta^{13}C$ values from compound-specific isotope analysis of amino acids (AAs) for essential (Ile=Isoleucine, Lys=Lysine, Leu=Leucine, Met=Methionine, Phe=Phenylalanine, Val=Valine) and non-essential (Ala=Alanine, Asp=Aspartame, Glu=Glutamate, Pro=Proline, Gly=Glycine) AAs for polar cod and saffron cod from 2017 and 2018. Separate principal component (PC) analyses using $\delta^{13}C$ from essential AAs for polar cod (b) and saffron cod (c) show specimens as points and standard length as symbol size. Percentages are amount of variability in the data explained by each PC axis.

562 Fish for CSIAA were primarily collected in the northern region of the study domain due
563 to fish presence and sample availability (Fig. 7). However, samples were collected from various
564 water masses that included regions with *Melt,* generally at the surface of the water column (Fig.
565 3), and regions with *Pacific* but not *Melt* (Fig. 7). The majority of the Chukchi was comprised of

Pacific during 2017, but many fish were located, and therefore collected, outside of the region where *Pacific* dominated the water column (Fig. 7). During 2018 when mean currents were southwestward (Fig. 4b), *Melt* and *Cold shelf* extended south (Fig. 7). While *Melt* and low salinity water from runoff and riverine sources cannot be definitively differentiated from temperature and salinity (Mueter et al. 2021), *Melt* was primarily present offshore and at high latitudes, supporting likely *Melt* influences (Fig. 7). Water mass spatial patterns also generally coincided with other studies in the region, although sampling did not cover very nearshore areas in the northern Chukchi that may be influenced by Pacific-origin water masses (Danielson et al. 2017; Marsh et al. 2017). Despite variation in water masses, spatial patterns in CSIAA showed minimal discernible patterns except for the inshore to offshore gradient of ^{13}C depletion to enrichment across Barrow Canyon (labeled in Fig. 1). This gradient coincided with multiple water masses across the canyon (Fig. 7).

578

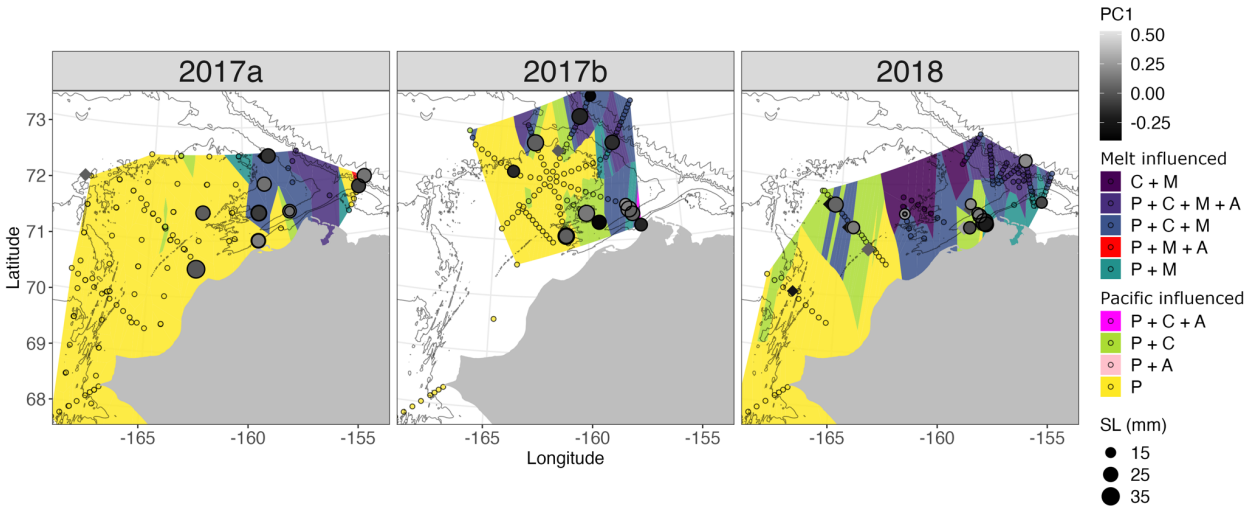

Figure 7. Water mass distributions and CSIAA sample locations from surveys in 2017 (2017a and 2017b) and 2018. Open circles are CTD stations where data were collected. Melt influenced refers to stations with *Melt* water present in the water column. Pacific influenced refers to stations with *Pacific* but no *Melt*. Colors show water masses that were present at each station within the top 200 m of the water column (see Fig. 3; C=*Cold shelf*, M=*Melt*, P=*Pacific*, A=*Atlantic*), with rarer water mass observations shown in shades of red for ease of interpretation. Water masses are mapped using Voronoi diagrams for visualization, warranting caution about interpretation of exact geographic transitions between water masses. Gray symbols are principal component axis 1 scores for polar cod (circles) and saffron cod (diamonds) from Fig. 6 and symbol size is standard length (SL).

579 Essential AA $\delta^{13}C$ values of polar cod were minimally influenced by the average local
580 physical environment (eq 5) except for a weak relationship with chl-*a* (Table 1). Essential AA
581 $\delta^{13}C$ was more strongly related to average chl-*a* in combination with whether sampling locations
582 were *Pacific* influenced or *Melt* influenced. Collection year also moderately improved the model
583 (Table 1). PC1 scores were generally greater (e.g. enriched essential AA $\delta^{13}C$) with increasing

584 chl-*a*, but were only linear for *Pacific* influenced locations (Fig. 8). The nonlinear relationship in
585 *Melt* influenced environments was not associated with particular combinations of water masses,
586 suggesting that more specific water mass factor levels in GAMs would likely not capture
587 additional relationships between water masses and essential AA $\delta^{13}C$ for polar cod. Within *Melt*
588 influenced waters, the highest chl-*a* and $\delta^{13}C$ were in 2018 and the lowest in 2017 (Fig. 8).

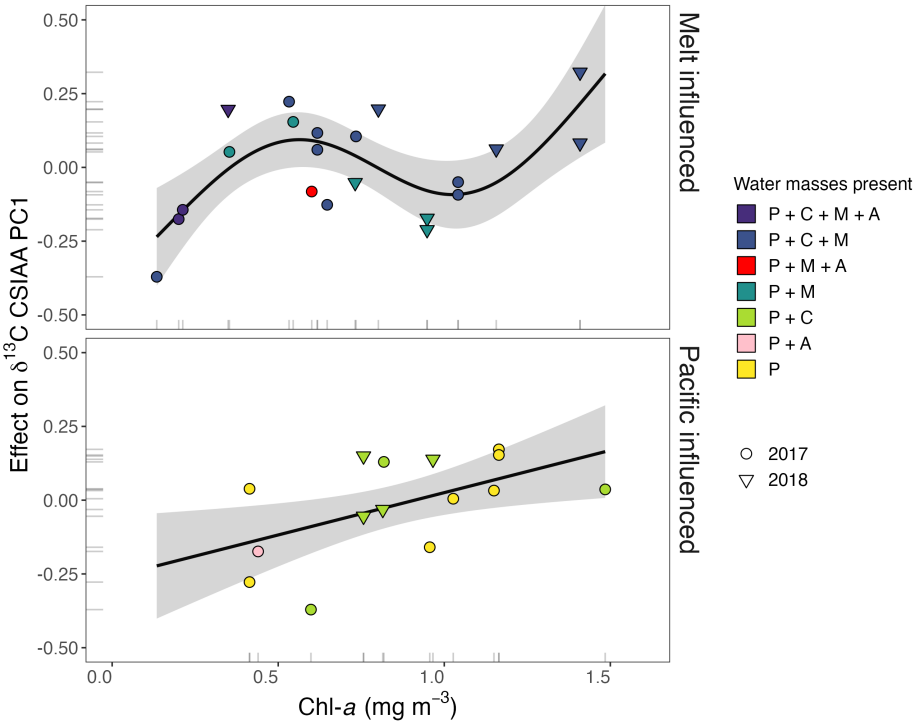

Figure 8. Generalized additive model results showing the effect of chl-*a* on $\delta^{13}C$ compound-specific isotope analysis of amino acid (CSIAA) principal component (PC) axis 1 scores for polar cod. Plots show separate smooths for *Melt* influenced and *Pacific* influenced stations with data points plotted against the smooth, where symbol shapes designate collection year and colors are the water masses present in the water column at each station (C=*Cold shelf*, M=*Melt*, P=*Pacific*, A=*Atlantic*; see Figs. 2 and 7). Confidence bands are ± two standard errors (gray shading) and whiskers are data values.

589

590

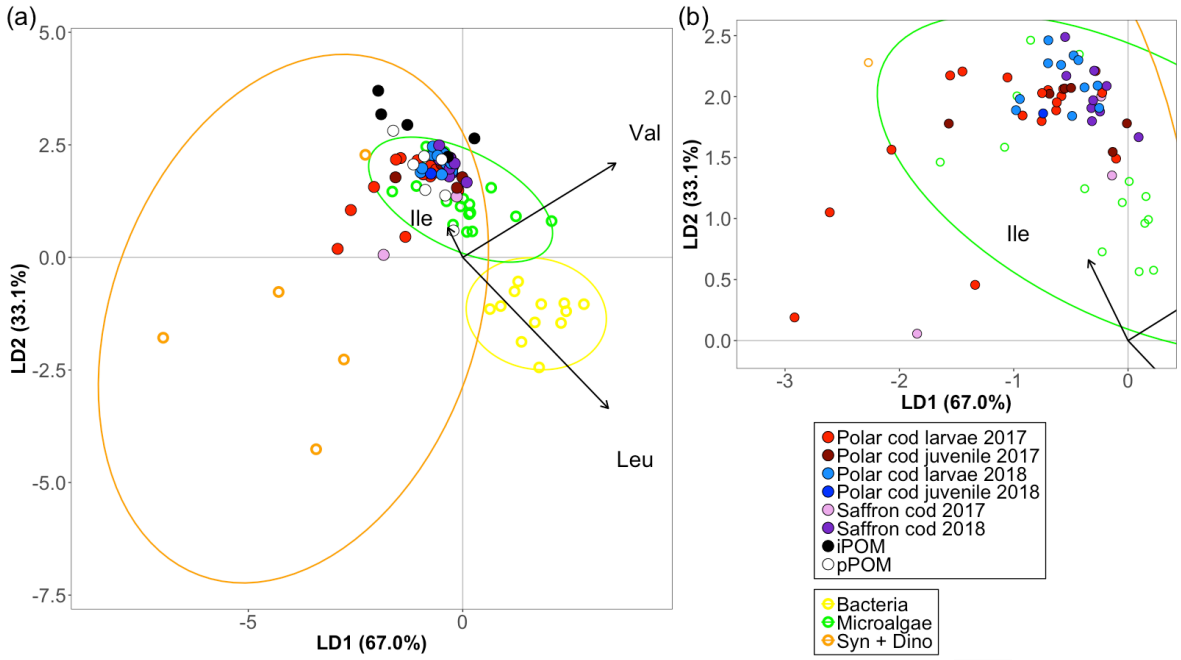

Figure 9. (a) Linear discriminant (LD) analysis of isotopic "fingerprints" of $\delta^{13}C$ essential amino acids (Ile=Isoleucine, Val=Valine, Leu=Leucine) from potential carbon sources (Bacteria, Microalgae, Syn + Dino; open circle points) and predictions (projections onto the linear discriminants) for polar cod, saffron cod, ice-associated particular organic matter (iPOM), and pelagic particulate organic matter (pPOM). (b) Truncated axes from (a) to show variation in predictions among fish. Microalgae included cryptophytes, chrysophytes, some genera of cyanobacteria, haptophytes, chlorophytes, and diatoms. Syn + Dino is *Synechococcoccus* and dinoflagellates. Axes show percentage of explained between-group variance and 95% confidence ellipses are shown. Points are color coded by LDA subgroup and correspond to specimens or literature-based values (Supplemental Table 1).

591

592 Gadid isotopic "fingerprints" ordinated closely with Microalgae (Fig 9 and Supplemental
593 Fig. 3) and were most similar to chrysophytes, diatoms, cryptophytes, pPOM, and fjord samples
594 due to ^{13}C enrichment of Val, particularly during 2018 (Supplemental Fig. 3 Supplemental Table
595 1). "Fingerprints" of both gadids were more similar to pPOM than iPOM (Fig 9 and
596 Supplemental Fig. 3). Phe ^{13}C enrichment was associated with dinoflagellates and
597 *Synechococcus*, and during 2017 Phe was ^{13}C-enriched for some polar cod larvae and saffron cod
598 (Figs. 6 and 9; Supplemental Fig. 3).

599 The LDA had an overall accuracy of 0.97 (Confidence Interval 0.85-1.00) with the lowest
600 correct classification for Syn + Dino (correct: 0.80, misclassified as Microalgae: 0.20) compared
601 to Microalgae (correct: 0.94, misclassified as Bacteria: 0.06) and Bacteria (correct: 1.00). LDA
602 group predictions for gadids suggested that carbon was primarily sourced from Microalgae with
603 potential contributions from either *Synechococcus* or dinoflagellates for some larval polar cod
604 and saffron cod during 2017 (Fig. 9). Additionally, pPOM primarily aligned with Microalgae,
605 whereas iPOM fell just outside the Microalgae designation, suggesting that iPOM reflects
606 additional primary producers. While iPOM was within the confidence ellipse of Syn + Dino,
607 isotope values of iPOM were ^{13}C-enriched for both Ile and Val, and the broad confidence ellipse
608 for Syn + Dino was primarily driven by a single data point (cross-referenced to *Synechococcus*
609 lab culture; Supplemental Table 1; Vokhshoori et al. 2014). This separation between pPOM,
610 iPOM, and Syn + Dino in combination with similarities between some gadid "fingerprints" in
611 2017 and Syn + Dino lends support to the inclusion of the three end members for isotope mixing
612 models.

The mixing models for Polar cod and saffron cod had high levels of uncertainty around most estimates, but carbon sources were primarily pPOM or iPOM followed by Syn + Dino (Figure 10). Uncertainty was potentially due to correlations between source proportions that can inflate marginal uncertainty in estimates of proportional contributions (Phillips et al., 2014). In particular, the strongest correlations were between iPOM and pPOM (-0.59 for polar cod and -0.55 for saffron cod models) that had wide posterior density distributions (Fig. 10). Additionally, posterior density distributions showing diet proportion estimates were sometimes multimodal (Fig. 10). Despite these limitations, clear patterns emerged. Diet proportion estimates for all polar cod combined and all saffron cod combined were broad, reflecting variation in diets among groups (years and life stages; Fig. 10). Polar cod larvae in 2018, polar cod juveniles, and saffron cod in both years primarily obtained carbon from pPOM, followed by iPOM. During 2017, both saffron cod and larval polar cod obtained some carbon from Syn + Dino, which was excluded from diets in 2018. Larval polar cod in 2017 also obtained a large proportion of carbon from iPOM (Fig 10). Unlike larvae, juvenile Polar cod carbon sources were almost entirely pPOM (Fig. 10).

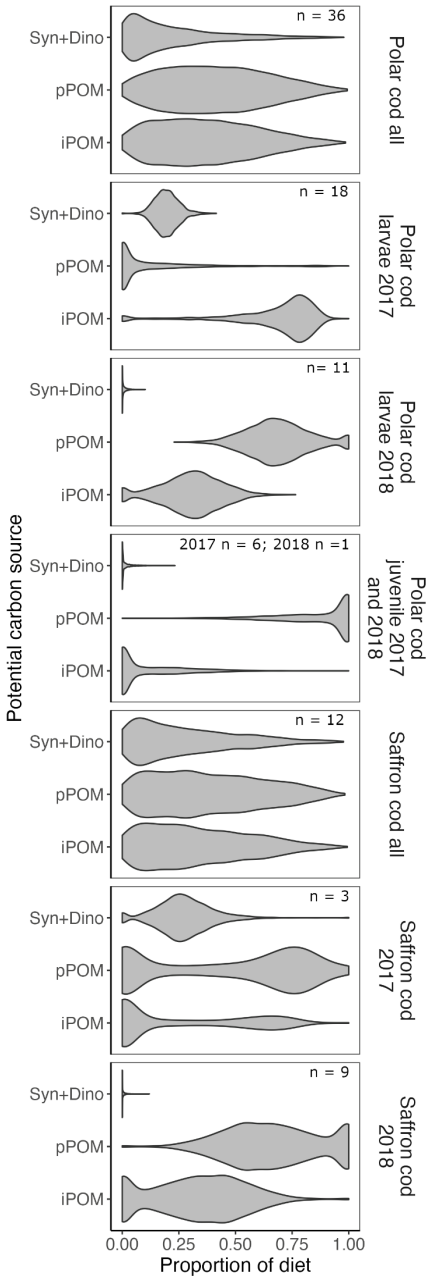

628

629 **Figure 10.** Scaled posterior density plots of diet estimates for forage fish from the Bayesian
630 mixing models for polar cod and saffron cod. Polar cod all and Saffron cod all refer to carbon
631 source contributions for all polar cod and saffron cod included in the species-specific models,
632 and subsequent groupings refer to year or age group combinations included as a random effects
633 in the models with sample size (n) presented for each.

Discussion

4.1 Spatial distributions

Distributions of pelagic lower trophic level organisms in the Chukchi were impacted by sea ice and open water, and secondarily influenced by wind reversals and current strength and direction. Concurrent with expected reliance on sympagic habitats, polar cod and *Calanus* were generally most prevalent at higher latitudes compared to *Pseudocalanus* and limited observations of saffron cod. Recent sea ice and earlier catch dates had positive relationships with *Calanus* abundance, underscoring life history connections with sea ice phenology and habitat use (Leu et al., 2011; Søreide et al., 2010). Direct relationships between recent sea ice and distributions differed for larval and juvenile polar cod. Larvae hatch under the ice (Bouchard and Fortier, 2008), but larval distributions were not influenced by recent sea ice and juveniles occurred more frequently in open water. Larvae at the time of collection may have remained in close proximity to hatch locations, resulting in distributions that were near to, or overlap with, regions of recent sea ice. In contrast, northward currents in ice free regions likely transported juvenile polar cod from southern locations (Deary et al., 2021; Vestfals et al., 2021), particularly later in the summer (positive impact of DOY) corresponding with growth throughout the season. Polar cod in the Chukchi have a protracted hatch window, creating the potential for co-occurring larvae and juveniles from multiple hatch dates and source locations (Chapman et al., 2023). Shared regions of high abundance of copepods and fish in the northeast near Hanna Shoal and Barrow Canyon support the role of transport and oceanographic convergence on distributions and pelagic ecosystem structure in the Chukchi. Aggregation hotspots also coincided with increased lipid content for polar cod (Copeman et al., 2022), hotspots for benthic organisms (Grebmeier et al., 2015), and northward currents that join near Hanna Shoal before exiting the shelf through

Barrow Canyon (Pickart et al., 2016; Stabeno et al., 2018). Accordingly, distributions are the result of phenology and habitat use that are mediated by sea ice presence, and currents in open water that promote mixing of southern and locally-sourced organisms.

Distributions during recent warm years support the combined influences of low sea ice, winds, and currents. During 2017, polar cod juveniles and, to a lesser degree, larvae were dispersed across the northern regions of the Chukchi shelf, *Pseudocalanus* abundance was low, and CPUE of *Calanus* was low. Absence of sea ice, weaker along-shelf currents, and frequent along-shelf wind reversals during 2017 differed markedly from other years. Under these unusual conditions, weaker currents potentially retained organisms on the shelf while frequent wind reversals dispersed water masses and organisms across the shelf (more uniform east-west distributions). This differs from most years when northward flows advect young fish off the shelf (Levine et al., 2021). Conditions in 2017 also contrasted with those in 2018 when ice retreated early but was present at concentrations that were not detected by satellites (Supplemental Fig. 10) compared to the complete lack of ice in the late summer in 2017 (E. D. Goldstein, *personal observation*). In contrast to 2017, directionality of currents in 2018 potentially pushed ice, *Melt* water, and associated organisms southwestward, leading to an east-west gradient in polar cod occurrence, and possibly increasing abundance of *Calanus*. Contrasts between the two years of early ice retreat highlight the substantial influences of winds and currents on pelagic ecosystem structure when sea ice extent is low.

Pseudocalanus distributions varied among years but were decoupled from sea ice, potentially due to habitat use or taxonomic resolution that combined species with differing habitats and life histories (Ershova et al. 2017). *Calanus* were also grouped by genera, but specimens were likely dominated by *C. glacialis* (Spear et al. 2019), resulting in a positive

680 relationship between sea ice and *Calanus* CPUE, and generally higher abundance at higher
681 latitudes. In contrast to surface-associated fish (Bouchard et al. 2016), *Calanus* and
682 *Pseudocalanus* CPUEs were low in 2017 and high in 2018. Abundances of both copepod taxa
683 may be related to depth-averaged currents (Runge and Ingram, 1991) that flowed northward in
684 2017 but shifted to the south in 2018.

685 ***4.2 Isotopic niche***

686 Sea ice was exceptionally low during both 2017 and 2018, but wind, currents, and
687 distributions of copepods and young forage fish differed. Despite being limited to only two years
688 of data, environmental distinctions between the low ice years suggest potential shifts in habitat,
689 diets, and basal resources of young fish. Polar cod had a broader isotopic niche during 2018 than
690 2017 that was primarily a result of a greater range of $\delta^{13}C$. Spatial patterns in $\delta^{13}C$ and ^{13}C
691 enrichment associated with northward transport through Bering Strait (Marsh et al., 2017; Schell
692 et al., 1998) suggest that the greater range of $\delta^{13}C$ was likely influenced by extensions of *Melt*
693 and *Cold shelf* waters farther south in 2018 due to a southwestward mean current direction.
694 Given the time lag of days to months associated with tissue integration (Vander Zanden et al.,
695 2015), differences in isotopic niche between years capture the influences of water mass diversity
696 and associated primary and secondary producers, as well as larval dispersal pathways. The
697 dominance of *Pacific* water and reduced isotopic niche for polar cod in 2017 coincided with
698 reduced lipid storage (Copeman et al., 2022), reflecting a shift in environmental and feeding
699 conditions and a more homogenous environment for a critical intermediary species in Arctic
700 food webs.

701 Isotopic niche variation between forage fish with differing tolerances to warming (Laurel
702 et al., 2016), different lipid profiles (Copeman et al., 2022), but similar functional roles in the

food web suggest that changes in species abundance could alter trophic pathways and energy transfer. Saffron cod had a narrower range of $\delta^{13}C$ and a greater range of $\delta^{15}N$ than polar cod. Young polar cod rely heavily on calanoid copepods, whereas saffron cod feed from a more diverse prey base (Bouchard and Fortier, 2020; Copeman et al., 2020). A narrower prey base for polar cod could limit trophic range, but have a lesser impact on $\delta^{13}C$ that is likely influenced by water masses to a greater degree than $\delta^{15}N$. Adult calanoid copepods comprise a small portion of young polar cod diets (Bouchard and Fortier, 2020), but greater variability in $\delta^{13}C$ than $\delta^{15}N$ between years for copepods was congruent with the pattern observed for polar cod. Sympagic food webs show greater modularity and sensitivity to change than other high-latitude food webs (Kortsch et al., 2019) and narrowing isotopic niche for polar cod could reflect such vulnerabilities.

4.3 Basal carbon sources

Young polar cod diets are coupled with ice-algal food webs, but strong linkages may be reduced in the absence of sea ice (Graham et al., 2014; Kohlbach et al., 2017). Polar cod were present during the summers of 2017 and 2018, but sea ice and *Melt* signatures were largely absent in 2017, suggesting that diets may be derived from alternative basal carbon sources. Essential AA $\delta^{13}C$ showed little correlation with body length (ontogeny) but diverged between years for both fish species. Spatial patterns were variable except for an inshore-offshore gradient across Barrow Canyon that also coincided with gradients in bulk $\delta^{13}C$ and transitions between water masses. This gradient lends support to oceanographic convergence of pelagic organisms and water masses at Barrow Canyon before they are funneled off the shelf, and suggests that carbon source contributions to fish diets were influenced by water masses with distinct plankton communities (Danielson et al., 2017; Logerwell et al., 2020).

Heterogeneous patterns in $\delta^{13}C$ across the majority of the shelf contradicts the influence of water masses on essential AA $\delta^{13}C$, but there are several factors that likely decouple direct relationships. (1) Habitat use: Water masses are depth-stratified but specimens were collected throughout the water column, precluding the ability to directly determine water mass occupancy. (2) Diet preference: Polar cod may selectively feed on copepod species (Bouchard and Fortier, 2020) that may also utilize variable habitats or have restricted diets, thus impacting essential AA $\delta^{13}C$ despite differences in plankton and prey composition among water masses. (3) Transport: Stable isotopes integrate diets over time, and the water mass from which a specimen was collected could differ from previously occupied habitats. (4) Phytoplankton composition and blooms: Essential AA $\delta^{13}C$ had a positive relationship with chl-*a* (a proxy for phytoplankton abundance or photosynthetic rates; Behrenfeld and Falkowski, 1997) but differed between *Pacific* and *Melt* influenced waters. These relationships suggest that primary producers differed among water masses and impacted $\delta^{13}C$, but coincides with alterations in $\delta^{13}C$ depending on growth of plankton or the progression of algal blooms (de la Vega et al., 2019). (5) Water mass designations: Temperature and salinity alone cannot definitively separate *Melt* waters at the surface from low salinity water derived from freshwater runoff (Mueter et al. 2021). Decoupling of essential AA $\delta^{13}C$ with spatial patterns in water masses and nonlinear relationships with chl-*a* in *Melt* influenced waters could be influenced by misclassified water masses given strict cutoffs for designations. Land-based freshwater or *Alaskan coastal* water influences should be greatest nearshore (Danielson et al. 2017; Marsh et al. 2017). *Melt* was primarily found offshore and at high latitudes in the Chukchi, lending credence to water mass designations.

Presumably loss of sea ice, lack of *Melt* water, and increases in *Pacific* water coincide with declines in sea ice algae and increases in pelagic phytoplankton. Sea ice algae is primarily

749 comprised of diatoms that are found in high concentrations in the northern Chukchi (Crawford et
750 al., 2018), but can include other groups of microalgae that are found in temperate and Arctic
751 environments (Supplemental Table 1; Neukermans et al., 2018; Schollmeier et al., 2018).
752 Essential AA $\delta^{13}C$ of both forage fish were indicative of carbon sourced primarily from
753 Microalgae, and indeed, pPOM coincided with Microalgae "fingerprints" and made the greatest
754 proportional contribution to fish diets. Notably, even in the low ice years, iPOM likely remained
755 a carbon source, or signatures were retained in tissues, for both fish species into the late summer.
756 Diet contributions for juvenile polar cod were almost entirely from pPOM, in agreement with a
757 reduced dependency on sea ice environments and greater presence in open water.
758 Exceptions to the high contribution of pPOM occurred during 2017 when ^{13}C Phe
759 enrichment and Val depletion suggested a greater contribution from *Synechocccus* or
760 dinoflagellates for some larval polar cod and saffron cod. In contrast to potentially ice-associated
761 taxa, the picoplankton *Synechocccus* is primarily found in the southern Chukchi in warmer
762 *Pacific* water (Lomas et al. 2021; Flombaum et al., 2013). *Alaskan Coastal* water intrusion into
763 the Chukchi also increases autotrophic dinoflagellate biomass (the "fingerprint" used a
764 dinoflagellate group; Supplemental Table 1; Lee et al., 2014; Zhang et al., 2013). *Pseudocalanus*
765 diets can shift from diatoms and dinoflagellates in the spring to cyanobacteria in the summer
766 (Peters et al., 2006), highlighting the potential for trophic cascades. Putative diet shifts during
767 2017 are corroborated by evidence for reductions in diatom- and *Calanus*-sourced fatty acids for
768 larger juvenile polar cod in 2017 compared to other years (Copeman et al., 2022). Surprisingly,
769 the diet proportion of iPOM was greater than pPOM for larval polar cod in 2017. Some
770 microalgae groups overlap between pelagic and sea-ice habitats, creating challenges when
771 differentiating between the two sources (Vane et al., 2023) and potentially contributing to the

uncertainty and bimodal posterior distributions in the mixing models. Alternatively, the dichotomy between a higher proportion of iPOM in some diets, but contributions from Syn + Dino in others might reflect wind-driven current reversals in 2017 and mixing of fish from various source locations. The higher carbon contribution of Syn + Dino to larval polar cod diets during 2017 indicates that exceptionally low sea ice and *Pacific* water over most of the Chukchi shelf can impact basal carbon sources, potentially integrating a primarily subarctic primary producer into Arctic food webs.

4.4 Conclusions

The comprehensive outcomes of early ice retreat on energy transfer and trophic links are largely unknown and may differ among Arctic regions based on evidence for adaptability (Graham et al., 2014), potentially positive (LeBlanc et al., 2019), and negative (Copeman et al., 2022) impacts on Arctic forage fish. In the Chukchi, the pelagic environment is largely influenced by sea ice, but as summer sea ice continues to decline, the influences of winds and currents on lower trophic levels become more evident. Summer of 2017 provided an example of the compounding effects of physical conditions that led to dominance of southern-origin water masses, altered distributions of lower trophic level taxa, decreased isotopic niche for polar cod, and shifted carbon sources of larval polar cod toward boreal-associated primary producers. Early ice retreat alters the extent of sea ice-associated habitats, with multiple impacts on lower trophic level taxa that suggest a homogenization of subarctic and Arctic shelf habitats, food webs, and ecosystems.

References

Akaike, H., 1998. Information Theory and an Extension of the Maximum Likelihood Principle,

in: Parzen, E., Tanabe, K., Kitagawa, G. (Eds.), Selected Papers of Hirotugu Akaike, Springer Series in Statistics. Springer, New York, NY, pp. 199–213. https://doi.org/10.1007/978-1-4612-1694-0_15

Axler, K.E., Goldstein, E.D., Nielsen, J.M., Deary, A.L., Duffy-Anderson, J.T., 2023. Shifts in the composition and distribution of Pacific Arctic larval fish assemblages in response to rapid ecosystem change. Global Change Biology gcb.16721. https://doi.org/10.1111/gcb.16721

Behrenfeld, M.J., Falkowski, P.G., 1997. Photosynthetic rates derived from satellite-based chlorophyll concentration. Limnol. Oceanogr. 1–20.

Bouchard, C., Fortier, L., 2020. The importance of *Calanus glacialis* for the feeding success of young polar cod: a circumpolar synthesis. Polar Biol. https://doi.org/10.1007/s00300-020-02643-0

Bouchard, C., Fortier, L., 2008. Effects of polynyas on the hatching season, early growth and survival of polar cod *Boreogadus saida* in the Laptev Sea. Mar. Ecol. Prog. Ser. 355, 247–256. https://doi.org/10.3354/meps07335

Bouchard, C., Mollard, S., Suzuki, K., Robert, D., Fortier, L., 2016. Contrasting the early life histories of sympatric Arctic gadids Boreogadus saida and Arctogadus glacialis in the Canadian Beaufort Sea. Polar Biol 39, 1005–1022. https://doi.org/10.1007/s00300-014-1617-4

Chapman, Z.M., Mueter, F.J., Norcross, B.L., Oxman, D.S., 2023. Arctic cod (Boreogadus saida) hatching season and growth rates in the Bering, Chukchi and Beaufort seas. Deep Sea Res. Part II Top. Stud. Oceanogr. 207, 105226. https://doi.org/10.1016/j.dsr2.2022.105226

Copeman, L.A., Salant, C.D., Stowell, M.A., Spencer, M.L., Kimmel, D.G., Pinchuk, A.I., Laurel, B.J., 2022. Annual and spatial variation in the condition and lipid storage of juvenile Chukchi Sea gadids during a recent period of environmental warming (2012 to 2019). Deep Sea Res. Part II Top. Stud. Oceanogr. 205, 105180. https://doi.org/10.1016/j.dsr2.2022.105180

Copeman, L., Spencer, M., Heintz, R., Vollenweider, J., Sremba, A., Helser, T., Logerwell, L., Sousa, L., Danielson, S., Pinchuk, A.I., Laurel, B., 2020. Ontogenetic patterns in lipid and fatty acid biomarkers of juvenile polar cod (*Boreogadus saida*) and saffron cod (*Eleginus gracilis*) from across the Alaska Arctic. Polar Biol. https://doi.org/10.1007/s00300-020-02648-9

Corlett, W. B., Pickart, R. S., 2017. The Chukchi slope current. Prog. Oceanogr. **153**: 50–65. doi:10.1016/j.pocean.2017.04.005

Crawford, D.W., Cefarelli, A.O., Wrohan, I.A., Wyatt, S.N., Varela, D.E., 2018. Spatial patterns in abundance, taxonomic composition and carbon biomass of nano- and microphytoplankton in Subarctic and Arctic Seas. Prog. Oceanogr. 162, 132–159. https://doi.org/10.1016/j.pocean.2018.01.006

Danielson, S.L., Eisner, L., Ladd, C., Mordy, C., Sousa, L., Weingartner, T.J., 2017. A comparison between late summer 2012 and 2013 water masses, macronutrients, and phytoplankton standing crops in the northern Bering and Chukchi Seas. Deep Sea Res. Part II Top. Stud. Oceanogr., Arctic Ecosystem Integrated Survey (Arctic Eis): Marine ecosystem dynamics in the rapidly changing Pacific Arctic Gateway 135, 7–26. https://doi.org/10.1016/j.dsr2.2016.05.024

840 Danielson, S.L., Weingartner, T.J., Hedstrom, K.S., Aagaard, K., Woodgate, R., Curchitser, E.,
841 Stabeno, P.J., 2014. Coupled wind-forced controls of the Bering–Chukchi shelf
842 circulation and the Bering Strait throughflow: Ekman transport, continental shelf waves,
843 and variations of the Pacific–Arctic sea surface height gradient. Prog. Oceanogr. 125, 40–
844 61. https://doi.org/10.1016/j.pocean.2014.04.006
845 de la Vega, C., Jeffreys, R.M., Tuerena, R., Ganeshram, R., Mahaffey, C., 2019. Temporal and
846 spatial trends in marine carbon isotopes in the Arctic Ocean and implications for food
847 web studies. Glob. Change Biol. 25, 4116–4130. https://doi.org/10.1111/gcb.14832
848 Deary, A.L., Vestfals, C.D., Mueter, F.J., Logerwell, E.A., Goldstein, E.D., Stabeno, P.J.,
849 Danielson, S.L., Hopcroft, R.R., Duffy-Anderson, J.T., 2021. Seasonal abundance,
850 distribution, and growth of the early life stages of polar cod (*Boreogadus saida*) and
851 saffron cod (*Eleginus gracilis*) in the US Arctic. Polar Biol. 44, 2055–2076.
852 https://doi.org/10.1007/s00300-021-02940-2
853 Docherty, G., Jones, V., Evershed, R. P., 2001. Practical and theoretical considerations in the gas
854 chromatography/combustion/isotope ratio mass spectrometry $\delta^{13}C$ analysis of small
855 polyfunctional compounds. Rapid Commun. Mass Spectrom. RCM 15: 730–738.
856 doi:10.1002/rcm.270
857 El-Sabaawi, R., Dower, J.F., Kainz, M., Mazumder, A., 2009. Characterizing dietary variability
858 and trophic positions of coastal calanoid copepods: insight from stable isotopes and fatty
859 acids. Mar. Biol. 156, 225–237. https://doi.org/10.1007/s00227-008-1073-1
860 Ershova, E.A., Questel, J.M., Kosobokova, K., Hopcroft, R.R., 2017. Population structure and
861 production of four sibling species of *Pseudocalanus* spp. in the Chukchi Sea. J. Plankton
862 Res. 39, 48–64. https://doi.org/10.1093/plankt/fbw078

863 Fasiolo, M., Nedellec, R., Goude, Y., Wood, S.N., 2020. Scalable Visualization Methods for
864 Modern Generalized Additive Models. J. Comput. Graph. Stat. 29, 78–86.
865 https://doi.org/10.1080/10618600.2019.1629942
866 Flombaum, P., Gallegos, J.L., Gordillo, R.A., Rincón, J., Zabala, L.L., Jiao, N., Karl, D.M., Li,
867 W.K.W., Lomas, M.W., Veneziano, D., Vera, C.S., Vrugt, J.A., Martiny, A.C., 2013.
868 Present and future global distributions of the marine Cyanobacteria *Prochlorococcus* and
869 *Synechococcus*. Proc. Natl. Acad. Sci. 110, 9824–9829.
870 https://doi.org/10.1073/pnas.1307701110
871 Fortier, L., Ponton, D., Gilbert, M., 1995. The match/mismatch hypothesis and the feeding
872 success of fish larvae in ice-covered southeastern Hudson Bay. Mar. Ecol. Prog. Ser. 120,
873 11–27. https://doi.org/10.3354/meps120011
874 Frainer, A., Primicerio, R., Kortsch, S., Aune, M., Dolgov, A.V., Fossheim, M., Aschan, M.M.,
875 2017. Climate-driven changes in functional biogeography of Arctic marine fish
876 communities. Proc. Natl. Acad. Sci. 114, 12202–12207.
877 https://doi.org/10.1073/pnas.1706080114
878 Graham, C., Oxtoby, L., Wang, S.W., Budge, S.M., Wooller, M.J., 2014. Sourcing fatty acids to
879 juvenile polar cod (*Boreogadus saida*) in the Beaufort Sea using compound-specific
880 stable carbon isotope analyses. Polar Biol. 37, 697–705. https://doi.org/10.1007/s00300-
881 014-1470-5
882 Gray, B.P., Norcross, B.L., Blanchard, A.L., Beaudreau, A.H., Seitz, A.C., 2016. Variability in
883 the summer diets of juvenile polar cod (*Boreogadus saida*) in the northeastern Chukchi
884 and western Beaufort Seas. Polar Biol. 39, 1069–1080. https://doi.org/10.1007/s00300-
885 015-1796-7

886 Grebmeier, J.M., 2012. Shifting Patterns of Life in the Pacific Arctic and Sub-Arctic Seas.
887 Annual Review of Marine Science 4, 63–78. https://doi.org/10.1146/annurev-marine-
888 120710-100926
889 Grebmeier, J.M., Bluhm, B.A., Cooper, L.W., Danielson, S.L., Arrigo, K.R., Blanchard, A.L.,
890 Clarke, J.T., Day, R.H., Frey, K.E., Gradinger, R.R., Kędra, M., Konar, B., Kuletz, K.J.,
891 Lee, S.H., Lovvorn, J.R., Norcross, B.L., Okkonen, S.R., 2015. Ecosystem characteristics
892 and processes facilitating persistent macrobenthic biomass hotspots and associated
893 benthivory in the Pacific Arctic. Prog. Oceanogr., Synthesis of Arctic Research (SOAR)
894 136, 92–114. https://doi.org/10.1016/j.pocean.2015.05.006
895 Grebmeier, J., McRoy, C., Feder, H., 1988. Pelagic-benthic coupling on the shelf of the northern
896 Bering and Chukchi Seas. I. Food supply source and benthic bio-mass. Mar. Ecol. Prog.
897 Ser. 48, 57–67. https://doi.org/10.3354/meps048057
898 Griffith, G.P., Hop, H., Vihtakari, M., Wold, A., Kalhagen, K., Gabrielsen, G.W., 2019.
899 Ecological resilience of Arctic marine food webs to climate change. Nat. Clim. Change 9,
900 868–872. https://doi.org/10.1038/s41558-019-0601-y
901 Hersbach, H., Bell, B., Berrisford, P., Hirahara, S., Horanyi, A. Munoz-Sabater, J., Nicolas, J.,
902 Peubey, C., Radu, R., Schepers, D., Simmons, A., Soci, C., Abdalla, S., Abellan, X.,
903 Balsamo, G., Bechtold, P., Biavati, G., Bidlot, J., Bonavita, M., De Chiara, G., Dahlgren,
904 P., Dee, D., Diamantakis, M., Dragani, R., Flemming, J., Forbes, R., Fuentes, M., Geer,
905 A., Haimberger, L, Healy, S., Hogan, R. J., Holm, E., Janiskova, M., Keeley, S.,
906 Laloyaux, P., Lopez, P., Lupu, C., Radnoti, G., de Rosnay, P., Rozum, I., Vamborg, F.,
907 Villaume, S., Thepaut, J.-N., 2020. The ERA5 global reanalysis. Q. J. R. Meteorol. Soc.
908 **146**:1999-2049. doi:10.1002/qj.3803

909 Hop, H., Gjøsæter, H., 2013. Polar cod (*Boreogadus saida*) and capelin (*Mallotus villosus*) as
910 key species in marine food webs of the Arctic and the Barents Sea. Mar. Biol. Res. 9,
911 878–894. https://doi.org/10.1080/17451000.2013.775458
912 Hopcroft, R.R., Kosobokova, K.N., Pinchuk, A.I., 2010. Zooplankton community patterns in the
913 Chukchi Sea during summer 2004. Deep Sea Res. Part II Top. Stud. Oceanogr. 57, 27–
914 39. https://doi.org/10.1016/j.dsr2.2009.08.003
915 Houde, E.D., 2016. Recruitment Variability, in: Fish Reproductive Biology. John Wiley & Sons,
916 Ltd, pp. 98–187. https://doi.org/10.1002/9781118752739.ch3
917 Jackson, A.L., Inger, R., Parnell, A.C., Bearhop, S., 2011. Comparing isotopic niche widths
918 among and within communities: SIBER - Stable Isotope Bayesian Ellipses in R: Bayesian
919 isotopic niche metrics. J. Anim. Ecol. 80, 595–602. https://doi.org/10.1111/j.1365-
920 2656.2011.01806.x
921 Ji, R., Jin, M., Varpe, Ø., 2013. Sea ice phenology and timing of primary production pulses in
922 the Arctic Ocean. Glob. Change Biol. 19, 734–741. https://doi.org/10.1111/gcb.12074
923 Kędra, M., Cooper, L.W., Zhang, M., Biasatti, D., Grebmeier, J.M., 2019. Benthic trophic
924 sensitivity to on-going changes in Pacific Arctic seasonal sea ice cover – Insights from
925 the nitrogen isotopic composition of amino acids. Deep Sea Res. Part II Top. Stud.
926 Oceanogr. 162, 137–151. https://doi.org/10.1016/j.dsr2.2019.01.002
927 Koch, C.W., Brown, T.A., Amiraux, R., Ruiz-Gonzalez, C., MacCorquodale, M., Yunda-Guarin,
928 G.A., Kohlbach, D., Loseto, L.L., Rosenberg, B., Hussey, N.E., Ferguson, S.H.,
929 Yurkowski, D.J., 2023. Year-round utilization of sea ice-associated carbon in Arctic
930 ecosystems. Nat Commun 14, 1964. https://doi.org/10.1038/s41467-023-37612-8

931 Kohlbach, D., Schaafsma, F.L., Graeve, M., Lebreton, B., Lange, B.A., David, C., Vortkamp,
932 M., Flores, H., 2017. Strong linkage of polar cod (*Boreogadus saida*) to sea ice algae-
933 produced carbon: Evidence from stomach content, fatty acid and stable isotope analyses.
934 Prog. Oceanogr. 152, 62–74. https://doi.org/10.1016/j.pocean.2017.02.003
935 Kortsch, S., Primicerio, R., Aschan, M., Lind, S., Dolgov, A.V., Planque, B., 2019. Food-web
936 structure varies along environmental gradients in a high-latitude marine ecosystem.
937 Ecography 42, 295–308. https://doi.org/10.1111/ecog.03443
938 Kortsch, S., Primicerio, R., Fossheim, M., Dolgov, A.V., Aschan, M., 2015. Climate change
939 alters the structure of arctic marine food webs due to poleward shifts of boreal
940 generalists. Proc. R. Soc. B Biol. Sci. 282, 20151546.
941 https://doi.org/10.1098/rspb.2015.1546
942 Larsen, T., Ventura, M., Andersen, N., O'Brien, D.M., Piatkowski, U., McCarthy, M.D., 2013.
943 Tracing carbon sources through aquatic and terrestrial food webs using amino acid stable
944 isotope fingerprinting. PLoS ONE 8, e73441.
945 https://doi.org/10.1371/journal.pone.0073441
946 Laurel, B.J., Spencer, M., Iseri, P., Copeman, L.A., 2016. Temperature-dependent growth and
947 behavior of juvenile Arctic cod (*Boreogadus saida*) and co-occurring North Pacific
948 gadids. Polar Biol. 39, 1127–1135. https://doi.org/10.1007/s00300-015-1761-5
949 LeBlanc, M., Geoffroy, M., Bouchard, C., Gauthier, S., Majewski, A., Reist, J.D., Fortier, L.,
950 2019. Pelagic production and the recruitment of juvenile polar cod *Boreogadus saida* in
951 Canadian Arctic seas. Polar Biol. https://doi.org/10.1007/s00300-019-02565-6

952 Lee, S.H., Dahms, H.-U., Kim, Y., Choy, E.J., Kang, S.-H., Kang, C.-K., 2014. Spatial
953 distribution of small phytoplankton composition in the Chukchi Sea. Polar Biol. 37, 99–
954 109. https://doi.org/10.1007/s00300-013-1413-6
955 Leu, E., Søreide, J.E., Hessen, D.O., Falk-Petersen, S., Berge, J., 2011. Consequences of
956 changing sea-ice cover for primary and secondary producers in the European Arctic shelf
957 seas: Timing, quantity, and quality. Prog. Oceanogr. 90, 18–32.
958 https://doi.org/10.1016/j.pocean.2011.02.004
959 Levine, R.M., De Robertis, A., Grünbaum, D., Woodgate, R., Mordy, C.W., Mueter, F., Cokelet,
960 E., Lawrence-Slavas, N., Tabisola, H., 2021. Autonomous vehicle surveys indicate that
961 flow reversals retain juvenile fishes in a highly advective high-latitude ecosystem.
962 Limnol. Oceanogr. 66, 1139–1154. https://doi.org/10.1002/lno.11671
963 Levinsen, H., Turner, J., Nielsen, T., Hansen, B., 2000. On the trophic coupling between protists
964 and copepods in Arctic marine ecosystems. Mar. Ecol. Prog. Ser. 204, 65–77.
965 https://doi.org/10.3354/meps204065
966 Logerwell, E.A., Busby, M., Mier, K.L., Tabisola, H., Duffy-Anderson, J., 2020. The effect of
967 oceanographic variability on the distribution of larval fishes of the northern Bering and
968 Chukchi seas. Deep Sea Res. Part II Top. Stud. Oceanogr., Understanding Ecosystem
969 Processes in the Pacific Arctic 177, 104784. https://doi.org/10.1016/j.dsr2.2020.104784
970 Lomas, M. W., Eisner, L., Nielsen, J. M., Danielson, S., Mordy, C. W., Stabeno, P. J., Laney, S.
971 R., 2021. Growing importance of *Synechococcus* abundance and biomass in the Northern
972 Bering and Chukchi seas. In: Stabeno, P. J., Axler, K., Copeman, L, Deary, A., Duffy-
973 Anderson, J. T., Eisner, L., Goldstein, E., Kimmel, D., Lomas, M. W., McCabe, R.,

974 Mordy, C. W., Nielsen, J. M., Spear, A. (Eds.), Arctic IES oceanography & lower trophic
975 levels (A92). NPRB Final Report. pp. 315-331.
976 Lorenzen, C., J., 1966. A method for the continuous measurement of in vivo chlorophyll
977 concentration. Deep Sea Res Oceanogr Abstr. 13: 223-227. doi:10.1016/0011-
978 7471(66)91102-8
979 Marsh, J.M., Mueter, F.J., Iken, K., Danielson, S., 2017. Ontogenetic, spatial and temporal
980 variation in trophic level and diet of Chukchi Sea fishes. Deep Sea Res. Part II Top. Stud.
981 Oceanogr. 135, 78–94. https://doi.org/10.1016/j.dsr2.2016.07.010
982 Matarese, A.C., Blood, D.M., Picquelle, S.J., Benson, J.L., 2003. Atlas of abundance and
983 distribution patterns of ichthyoplankton from the Northeast Pacific Ocean and Bering Sea
984 ecosystems: based on research conducted by the Alaska Fisheries Science Center (1972–
985 1996) [WWW Document]. URL http://spo.nwr.noaa.gov/pp1.pdf (accessed 12.29.16).
986 McMahon, K.W., Fogel, M.L., Elsdon, T.S., Thorrold, S.R., 2010. Carbon isotope fractionation
987 of amino acids in fish muscle reflects biosynthesis and isotopic routing from dietary
988 protein: Carbon isotope fractionation of fish muscle amino acids. J. Anim. Ecol. 79,
989 1132–1141. https://doi.org/10.1111/j.1365-2656.2010.01722.x
990
991 Mueter, F., Iken, K., Cooper, L., Grebmeier, J., Kuletz, K., Hopcroft, R., Danielson, S., Collins,
992 E., Cushing, D., 2021. Changes in diversity and species composition across multiple
993 assemblages in the eastern Chukchi Sea during two contrasting years are consistent with
994 borealization. Oceanog 34. https://doi.org/10.5670/oceanog.2021.213
995 Mueter, F.J., Nahrgang, J., John Nelson, R., Berge, J., 2016. The ecology of gadid fishes in the
996 circumpolar Arctic with a special emphasis on the polar cod (*Boreogadus saida*). Polar
997 Biology 39, 961–967. https://doi.org/10.1007/s00300-016-1965-3

Michaud, J.E., Fortier, L., Rowe, P., Ramseier, R., 1996. Feeding success and survivorship of Arctic cod larvae, *Boreogadus saida*, in the Northeast Water polynya (Greenland Sea). Fish. Oceanogr. 5, 120–135. https://doi.org/10.1111/j.1365-2419.1996.tb00111.x

Neukermans, G., Oziel, L., Babin, M., 2018. Increased intrusion of warming Atlantic water leads to rapid expansion of temperate phytoplankton in the Arctic. Glob. Change Biol. 24, 2545–2553. https://doi.org/10.1111/gcb.14075

Ohkouchi, N., Chikaraishi, Y., Close, H.G., Fry, B., Larsen, T., Madigan, D.J., McCarthy, M.D., McMahon, K.W., Nagata, T., Naito, Y.I., Ogawa, N.O., Popp, B.N., Steffan, S., Takano, Y., Tayasu, I., Wyatt, A.S.J., Yamaguchi, Y.T., Yokoyama, Y., 2017. Advances in the application of amino acid nitrogen isotopic analysis in ecological and biogeochemical studies. Organic Geochemistry 113, 150–174. https://doi.org/10.1016/j.orggeochem.2017.07.009

Peters, J., Renz, J., van Beusekom, J., Boersma, M., Hagen, W., 2006. Trophodynamics and seasonal cycle of the copepod *Pseudocalanus acuspes* in the Central Baltic Sea (Bornholm Basin): evidence from lipid composition. Mar. Biol. 149, 1417–1429. https://doi.org/10.1007/s00227-006-0290-8

Phillips, D.L., Inger, R., Bearhop, S., Jackson, A.L., Moore, J.W., Parnell, A.C., Semmens, B.X., Ward, E.J., 2014. Best practices for use of stable isotope mixing models in food-web studies. Can. J. Zool. 92, 823–835. https://doi.org/10.1139/cjz-2014-0127

Pickart, R.S., Moore, G.W.K., Mao, C., Bahr, F., Nobre, C., Weingartner, T.J., 2016. Circulation of winter water on the Chukchi shelf in early summer. Deep Sea Res. Part II Top. Stud. Oceanogr., More from NASA's ICESCAPE (Impacts of Climate on EcoSystems and

Chemistry of the Arctic Pacific Environment) program, Part 2 130, 56–75. https://doi.org/10.1016/j.dsr2.2016.05.001

Post, D.M., Layman, C.A., Arrington, D.A., Takimoto, G., Quattrochi, J., Montaña, C.G., 2007. Getting to the fat of the matter: models, methods and assumptions for dealing with lipids in stable isotope analyses. Oecologia 152, 179–189. https://doi.org/10.1007/s00442-006-0630-x

R Core Team (2017) R: a language and environment for statistical computing. R Foundation for Statistical Computing, Vienna

Rogachev, K.A., Carmack, E.C., Foreman, M.G.G., 2008. Bowhead whales feed on plankton concentrated by estuarine and tidal currents in Academy Bay, Sea of Okhotsk. Continental Shelf Research 28, 1811–1826. https://doi.org/10.1016/j.csr.2008.04.014

Rowe, A.G., Iken, K., Blanchard, A.L., O'Brien, D.M., Døving Osvik, R., Uradnikova, M., Wooller, M.J., 2019. Sources of primary production to Arctic bivalves identified using amino acid stable carbon isotope fingerprinting. Isotopes Environ. Health Stud. 55, 366–384. https://doi.org/10.1080/10256016.2019.1620742

Runge, J.A., Ingram, R.G., 1991. Under-ice feeding and diel migration by the planktonic copepods *Calanus glacialis* and *Pseudocalanus minutus* in relation to the ice algal production cycle in southeastern Hudson Bay, Canada. Mar. Biol. 108, 217–225. https://doi.org/10.1007/BF01344336

Schell, D., Barnett, B., Vinette, K., 1998. Carbon and nitrogen isotope ratios in zooplankton of the Bering, Chukchi and Beaufort seas. Mar. Ecol. Prog. Ser. 162, 11–23. https://doi.org/10.3354/meps162011

1044 Schollmeier, T., Oliveira, A.C.M., Wooller, M.J., Iken, K., 2018. Tracing sea ice algae into
1045 various benthic feeding types on the Chukchi Sea shelf. Polar Biol. 41, 207–224.
1046 https://doi.org/10.1007/s00300-017-2182-4
1047 Serreze, M.C., Barry, R.G., 2011. Processes and impacts of Arctic amplification: A research
1048 synthesis. Glob. Planet. Change 77, 85–96.
1049 https://doi.org/10.1016/j.gloplacha.2011.03.004
1050 Søreide, J.E., Carroll, M.L., Hop, H., Ambrose, W.G., Hegseth, E.N., Falk-Petersen, S., 2013.
1051 Sympagic-pelagic-benthic coupling in Arctic and Atlantic waters around Svalbard
1052 revealed by stable isotopic and fatty acid tracers. Mar. Biol. Res. 9, 831–850.
1053 https://doi.org/10.1080/17451000.2013.775457
1054 Søreide, J.E., Leu, E., Berge, J., Graeve, M., Falk-Petersen, S., 2010. Timing of blooms, algal
1055 food quality and *Calanus glacialis* reproduction and growth in a changing Arctic. Glob.
1056 Change Biol. 16, 3154–3163. https://doi.org/10.1111/j.1365-2486.2010.02175.x
1057 Spear, A., Duffy-Anderson, J., Kimmel, D., Napp, J., Randall, J., Stabeno, P., 2019. Physical and
1058 biological drivers of zooplankton communities in the Chukchi Sea. Polar Biol. 42, 1107–
1059 1124. https://doi.org/10.1007/s00300-019-02498-0
1060 Stabeno, P., Kachel, N., Ladd, C., Woodgate, R., 2018. Flow patterns in the eastern Chukchi Sea:
1061 2010-2015. J. Geophys. Res. Oceans 123, 1177–1195.
1062 https://doi.org/10.1002/2017JC013135
1063 Stabeno, P. J., McCabe, R. M., 2023. Re-examining flow pathways over the Chukchi Sea
1064 continental shelf, Deep Sea Res. Part II Top. Stud. Oceanogr. 207, 105243.
1065 doi:10.1016/j.dsr2.2022.105243.

1066 Stock, B.C., Jackson, A.L., Ward, E.J., Parnell, A.C., Phillips, D.L., Semmens, B.X., 2018.
1067 Analyzing mixing systems using a new generation of Bayesian tracer mixing models.
1068 PeerJ 6. https://doi.org/10.7717/peerj.5096
1069 Stock, B.C., Semmens, B.X., 2018. MixSIAR GUI user manual version 3.1.
1070 https://github.com/brianstock/MixSIAR/.
1071 Stock, B.C., Semmens, B.X., 2016. Unifying error structures in commonly used biotracer mixing
1072 models. Ecology 97, 2562–2569. https://doi.org/10.1002/ecy.1517
1073 Tedesco, L., Vichi, M., Scoccimarro, E., 2019. Sea-ice algal phenology in a warmer Arctic. Sci.
1074 Adv. 5, eaav4830. https://doi.org/10.1126/sciadv.aav4830
1075 Vander Zanden, M.J., Clayton, M.K., Moody, E.K., Solomon, C.T., Weidel, B.C., 2015. Stable
1076 isotope turnover and half-life in animal tissues: A literature synthesis. PLoS ONE 10.
1077 https://doi.org/10.1371/journal.pone.0116182
1078 Vane, K., Cobain, M.R.D., Trueman, C.N., Vonnahme, T.R., Rokitta, S., Polunin, N.V.C.,
1079 Flores, H., 2023. Tracing basal resource use across sea-ice, pelagic, and benthic habitats
1080 in the early Arctic spring food web with essential amino acid carbon isotopes. Limnology
1081 and Oceanography 68, 862–877. https://doi.org/10.1002/lno.12315
1082 Vargas, C., González, H., 2004. Plankton community structure and carbon cycling in a coastal
1083 upwelling system. I. Bacteria, microprotozoans and phytoplankton in the diet of copepods
1084 and appendicularians. Aquat. Microb. Ecol. 34, 151–164.
1085 https://doi.org/10.3354/ame034151
1086 Vestfals, C.D., Mueter, F.J., Duffy-Anderson, J.T., Busby, M.S., De Robertis, A., 2019. Spatio-
1087 temporal distribution of polar cod (*Boreogadus saida*) and saffron cod (*Eleginus gracilis*)

early life stages in the Pacific Arctic. Polar Biol. 42, 969–990. https://doi.org/10.1007/s00300-019-02494-4

Vestfals, C.D., Mueter, F.J., Hedstrom, K.S., Laurel, B.J., Petrik, C.M., Duffy-Anderson, J.T., Danielson, S.L., 2021. Modeling the dispersal of polar cod (*Boreogadus saida*) and saffron cod (*Eleginus gracilis*) early life stages in the Pacific Arctic using a biophysical transport model. Prog. Oceanogr. 196, 102571. https://doi.org/10.1016/j.pocean.2021.102571

Vokhshoori, N., Larsen, T., McCarthy, M., 2014. Reconstructing $\delta^{13}C$ isoscapes of phytoplankton production in a coastal upwelling system with amino acid isotope values of littoral mussels. Mar. Ecol. Prog. Ser. 504, 59–72. https://doi.org/10.3354/meps10746

von Quillfeldt, C.H., Ambrose, W.G., Clough, L.M., 2003. High number of diatom species in first-year ice from the Chukchi Sea. Polar Biol. 26, 806–818. https://doi.org/10.1007/s00300-003-0549-1

Walsh, R.G., He, S., Yarnes, C.T., 2014. Compound-specific $\delta^{13}C$ and $\delta^{15}N$ analysis of amino acids: a rapid, chloroformate-based method for ecological studies: GC/C/IRMS of chloroformate-derivatized amino acids. Rapid Commun. Mass Spectrom. 28, 96–108. https://doi.org/10.1002/rcm.6761

Wassmann, P., Reigstad, M., 2011. Future Arctic ocean seasonal ice zones and implications for pelagic-benthic coupling. Oceanography 24, 220–231. https://doi.org/10.5670/oceanog.2011.74

Whiteman, J., Elliott Smith, E., Besser, A., Newsome, S., 2019. A guide to using compound-specific stable isotope analysis to study the fates of molecules in organisms and ecosystems. Diversity 11, 8. https://doi.org/10.3390/d11010008

Wood, S., 2006. Generalized additive models: an introduction with R. CRC press.

Woodgate, R.A., Aagaard, K., Weingartner, T.J., 2005. Monthly temperature, salinity, and transport variability of the Bering Strait through flow. Geophys. Res. Lett. 32. https://doi.org/10.1029/2004GL021880

Zinkann, A.-C., Wooller, M.J., Leigh, M.B., Danielson, S., Gibson, G., Iken, K., 2022. Depth distribution of organic carbon sources in Arctic Chukchi Sea sediments. Deep Sea Research Part II: Topical Studies in Oceanography 199, 105076. https://doi.org/10.1016/j.dsr2.2022.105076

Zhang, F., He, J., Lin, L., Liu, Y., Wang, X., Ding, C., 2013. Spatial distribution of pico- and nano-phytoplankton and bacteria in the Chukchi Sea in relation to water masses: Spatial distribution of pico- and nano-phytoplankton and bacteria in the Chukchi Sea in relation to water masses. Adv. POLAR Sci. 23, 237–243. https://doi.org/10.3724/SP.J.1085.2012.00237

Zuur, A.F. (Ed.), 2009. Mixed effects models and extensions in ecology with R, Statistics for biology and health. Springer, New York, NY.

Acknowledgments

We are grateful for the expertise and insightful reviews of this manuscript provided by Dan Cooper and Brittany Schwarzkopf in addition to the thoughtful comments of two anonymous reviewers. We thank the Plankton Sorting and Identification Center in Szczecin, Poland, and the ichthyoplankton and zooplankton teams at the Alaska Fisheries Science Center for their taxonomic expertise that makes studies of the ecology of Arctic fishes and zooplankton possible. This project was funded by the North Pacific Research Board (NPRB), which sponsored the

Arctic Integrated Ecosystem Research Program (AIERP). Additional funding was received from NOAA's Ecosystems and Fisheries-Oceanography Coordinated Investigations Program (EcoFOCI) and from the Arctic Research Program, NOAA Research. Esther Goldstein was partially supported by The National Academies of Sciences, Engineering, and Medicine, National Research Council (NRC) Research Associateship Programs. This is NOAA PMEL Contribution number 5544, EcoFOCI Contribution EcoFOCI-1042, and NPRB Publication Number ArcticIERP-52. The findings and conclusions in the paper are those of the authors and do not necessarily represent the views of the National Marine Fisheries Service, NOAA. Reference to trade names does not imply endorsement by the National Marine Fisheries Service, NOAA.

Conflict of Interest

None declared.